INVESTIGATION OF PROTEIN CORONA FORMATION ON BIODEGRADABLE NANOCARRIERS

by

Damla Kelle

B.S., in Bioengineering, Yıldız Technical University, 2021

Submitted to the Institute of Biomedical Engineering
in partial fulfillment of the requirements
for the degree of
Master of Science
in
Biomedical Engineering

Boğaziçi University
2023

INVESTIGATION OF PROTEIN CORONA FORMATION ON BIODEGRADABLE NANOCARRIERS

APPROVED BY:

Assist. Prof. Dr. Banu İyisan .....
(Thesis Advisor)

Prof. Dr. Bora Garipcan .....

Assoc. Prof. Dr. Batur Ercan .....

DATE OF APPROVAL: 09.01.2023

ACKNOWLEDGMENTS

I would like to express my deepest gratitude to my advisor, Assist. Prof. Dr. Banu İYİSAN, for giving me a chance to be a part of this project and also for her support, guidance, and encouragement. She always taught me to look from a different perspective, not to give up, and to find the motivation to create a new solution in challenging situations. I appreciate the brainstorming and discussions we had together throughout my work.

I would like to thank Prof. Dr. Katharina LANDFESTER with my gratitude for giving me the opportunity to gain experience and improve myself further by allowing me to do my internship within her group.

I am grateful to all BiND Lab members; especially Dilan AVŞAR-AKDENİZ for her support and assistance; Sedef SALEL, Yağmur ZENGİN, Gizem UYSAL, Elif Özlem TOPAL for their friendship and making difficult days fun.

I am thankful to all members of Physical Chemistry of Polymers group; especially to Dr. María MARTINEZ-NEGRO, Dr. Sharafudheen Pottanam CHALI and Francesca MAZZOTTA for their guidance and support; Carina JUNG, Sarah LEMBKE, Dr. Marina MELCHIORS and Maria MICHEVA for their friendship and enjoyable talks; Kai SPETH for his support in liquid chromatography-mass spectrometry analysis, Gunnar GLASSER for his help in SEM imaging and Christoph SIEBER for his assistance in TEM imaging, Jennifer OBERLÄNDER and Iain HARLEY for their cooperation. I consider myself very lucky for the time we spent together at lunches, coffee breaks, and events organized.

Last but not least, I would like to thank my parents for believing in me even when I do not believe in myself, for their endless support to motivate me and trying to do their best for me. I am grateful to my beloved sister Dolunay KELLE who patiently

answers all of my scientific questions, always supports me in my most difficult times, and makes the greatest contribution to my personal development. I am very lucky that she is always there for me.

Human plasma experiments were conducted at Max Planck Institute for Polymer Research, Mainz, Germany by approval of the local ethics committee "Landesärztekammer Rheinland-Pfalz" [Bearbeitungsnummer: 837.439.12 (8540-F)].

This study was supported by the Scientific&Technological Research Council of Turkey (TÜBİTAK) (Project Number 121C205), Erasmus+ Programme of European Union and MPI for Polymer Research.

ACADEMIC ETHICS AND INTEGRITY STATEMENT

I, Damla Kelle, hereby certify that I am aware of the Academic Ethics and Integrity Policy issued by the Council of Higher Education (YÖK) and I fully acknowledge all the consequences due to its violation by plagiarism or any other way.

Name :

Signature:

Date:

ABSTRACT

INVESTIGATION OF PROTEIN CORONA FORMATION ON BIODEGRADABLE NANOCARRIERS

Biodegradable nanocarrier systems are significant tools for drug delivery systems since they enable prolonging the therapeutic effect of the chemotherapeutic drug by extending the release over a longer period of time. However, the most significant challenge of these systems is the protein corona (PC), the layer formed around the surface of nanocarriers by the adhesion of plasma proteins when nanocarriers are injected into the body intravenously. Since the PC structure identifies the nanocarriers' destiny in the body, it is required to be analyzed the proteins that form the PC structure comprehensively. In this study, proteins found in the hard protein corona (HPC) structure of two different biodegradable nanospheres (NSs), poly(lactide-co-glycolide) (PLGA) and polycaprolactone (PCL) NSs, were identified. For this purpose, distinct PLGA and PCL nanoparticles (NPs) were fabricated by miniemulsion/solvent evaporation method, followed by the characterization by electron microscopy, dynamic light scattering (DLS) and electrophoretic light scattering (ELS). Subsequently, PLGA and PCL NSs were treated with human plasma or FBS to form PC structure. Proteins in PC structures were analyzed by sodium dodecyl sulfate polyacrylamide gel electrophoresis. Furthermore, each protein in the HPC structure were identified by liquid chromatography-mass spectrometry (LC-MS) and grouped according to their functions. Moreover, doxorubicin hydrochloride, a significant chemotherapeutic drug, was encapsulated into PLGA NSs. Drug encapsulated NSs were characterized by DLS and ELS. Afterward, the PC structure around the surface of drug encapsulated NSs was formed by treating with human plasma or FBS. The impact of the PC on the drug release behavior of PLGA NSs was investigated at pH 7.4, a critical pH value to mimic the physiological environment.

Keywords: Biodegradable Nanocarriers, Polymer Nanoparticles, Protein Corona

ÖZET

BİYOBOZUNUR NANOTAŞIYICILARDA PROTEİN KORONA OLUŞUMUNUN İNCELENMESİ

Biyobozunur nanotaşıyıcı sistemler kemoterapötik ilacın salımını daha uzun bir süreye yayarak terapötik etkinin artmasını sağladığından ilaç taşıyıcı sistemler için önemli araçlardır. Fakat bu sistemlerin en önemli zorluğu, nanotaşıyıcıların intravenöz şekilde vücuda enjekte edilmesiyle plazma proteinlerinin yapışarak nanotaşıyıcıların yüzeyi etrafındaki tabaka olan protein koronanın (PC) oluşumudur. PC yapısı, nanotaşıyıcıların vücuttaki kaderini belirlediği için bu yapıyı oluşturan proteinlerin kapsamlı bir şekilde analiz edilmesi gerekmektedir. Bu çalışmada, iki farklı biyobozunur nanopartikül olan PLGA ve PCL nanopartiküllerinin kuvvetli bağlı protein korona (HPC) yapısındaki proteinlerinin belirlenmesine odaklanılmıştır. Bu amaçla, miniemülsiyon/çözücü buharlaştırma yöntemiyle farklı PLGA ve PCL nanopartikülleri sentezlendi; ardından dinamik ışık saçılımı (DLS), elektroforetik ışık saçılımı (ELS) ve elektron mikroskobu ile karakterizasyonları yapıldı. Daha sonra PLGA ve PCL nanoküreleri PC yapısının oluşması için insan plazması ya da FBS ile muamele edildi. Buna takiben, nanoküreler yüzeyinde oluşan PC yapısındaki proteinlerin analizi, sodyum dodesil sülfat poliakrilamid jel elektroforezi (SDS-PAGE) ile yapıldı. Ayrıca HPC yapısındaki proteinler, sıvı kromatografi-kütle spektrometrisi (LC-MS) ile belirlendi ve fonksiyonlarına göre gruplandırıldı. Ayrıca önemli bir kemoterapötik ilaç olan doksorubisin hidroklorür, PLGA nanokürelerinin içine enkapsüle edilmiştir. İlaç enkapsüle edilmiş nanoküreler, DLS ve ELS ile karakterize edildi. Ardından insan plazması ya da FBS ile muamele edilerek ilaç enkapsüle edilmiş nanokürelerin yüzeyinde PC yapısı oluşturuldu. PC'nin PLGA nanokürelerinin ilaç salım davranışı üzerindeki etkisi, fizyolojik ortamı taklit etmek için kritik bir pH değeri olan pH 7.4'te araştırıldı.

Anahtar Sözcükler: Biyobozunur Nanotaşıyıcılar, Polimer Nanopartiküller, Protein Korona

TABLE OF CONTENTS

ACKNOWLEDGMENTS . . . iii
ACADEMIC ETHICS AND INTEGRITY STATEMENT . . . v
ABSTRACT . . . vi
ÖZET . . . vii
LIST OF FIGURES . . . xii
LIST OF TABLES . . . xiv
LIST OF SYMBOLS . . . xvi
LIST OF ABBREVIATIONS . . . xvii
1. INTRODUCTION . . . 1
1.1 Motivation . . . 1
1.2 Objectives . . . 2
1.3 Thesis Outline . . . 2
2. RESEARCH BACKGROUND . . . 3
2.1 Cancer . . . 3
2.2 Nanocarrier Systems . . . 3
2.2.1 Physico-chemical Properties of Nanocarriers . . . 5
2.2.1.1 Size . . . 5
2.2.1.2 Shape . . . 5
2.2.1.3 Surface Properties . . . 6
2.2.2 Drug Targeting . . . 6
2.2.2.1 Active Targeting . . . 7
2.2.2.2 Passive Targeting . . . 8
2.3 Polymeric Nanocarriers . . . 9
2.3.1 Poly(lactic-co-glycolic acid) (PLGA) . . . 10
2.3.2 Polycaprolactone (PCL) . . . 11
2.4 Protein Corona . . . 12
2.4.1 Structure of Protein Corona . . . 13
2.4.2 Types of Proteins in Protein Corona . . . 14
2.4.3 Characterization of Protein Corona . . . 14

3. METHODS 16
3.1 Materials 16
3.2 Methods 17
3.2.1 Synthesis of Nanoparticles 17
3.2.2 Encapsulation of Doxorubicin into Nanoparticles 18
3.2.3 Characterization of Nanoparticles 19
3.2.3.1 Solid Content Analysis 19
3.2.3.2 Size and Polydispersity Index Measurement 19
3.2.3.3 Zeta Potential Analysis 19
3.2.3.4 Morphological Characterization 20
3.2.3.5 Centrifugation 20
3.2.3.6 Determination of Encapsulation Efficiency 20
3.2.4 Protein Corona Formation 21
3.2.5 Analysis of Protein Corona Structure 23
3.2.5.1 Protein Assay 23
3.2.5.2 SDS-PAGE 23
3.2.5.3 Silver Staining 24
3.2.5.4 Protein Digestion in Solution 25
3.2.5.5 Liquid Chromatography-Mass Spectrometry 25
3.2.6 *In vitro* Release of Doxorubicin 26
3.2.6.1 Doxorubicin Calibration Curve 26
3.2.6.2 Drug Release Analysis 26
4. RESULTS and DISCUSSION 28
4.1 Characterization Results of PLGA Nanoparticles 28
4.1.1 Solid Content Analysis 28
4.1.2 Size and Polydispersity Index Measurement 29
4.1.3 Zeta Potential Analysis 30
4.1.4 Morphological Characterization 30
4.1.5 Centrifugation 32
4.1.6 Solid Content Analysis of Centrifuged Nanoparticles 33
4.2 Characterization Results of PCL Nanoparticles 33
4.2.1 Solid Content Analysis 33

4.2.2 Size and Polydispersity Index Measurement 34
4.2.3 Zeta Potential Analysis 34
4.2.4 Morphological Characterization 35
4.2.5 Centrifugation 36
4.2.6 Solid Content Analysis of Centrifuged Samples 37
4.3 Analysis of Protein Corona on PLGA Nanospheres 37
4.3.1 Size and Polydispersity Index Measurement 38
4.3.2 Zeta Potential Analysis 39
4.3.3 Protein Assay 39
4.3.4 SDS-PAGE 40
4.3.5 Liquid Chromatography-Mass Spectrometry 42
4.4 Analysis of Protein Corona on PCL Nanospheres 44
4.4.1 Size and Polydispersity Index Measurement 45
4.4.2 Zeta Potential Analysis 45
4.4.3 Protein Assay 46
4.4.4 SDS-PAGE 47
4.4.5 Liquid Chromatography-Mass Spectrometry 48
4.5 Doxorubicin Encapsulated PLGA Nanospheres 50
4.5.1 Characterization of Doxorubicin Encapsulated PLGA Nanospheres 51
4.5.1.1 Solid Content Analysis 51
4.5.1.2 Size and Polydispersity Index Measurement 51
4.5.1.3 Zeta Potential Analysis 52
4.5.1.4 Determination of Encapsulation Efficiency 52
4.5.2 Analysis of Protein Corona on Doxorubicin Encapsulated PLGA Nanospheres 53
4.5.2.1 Size and Polydispersity Index Measurement 53
4.5.2.2 Zeta Potential Analysis 54
4.5.2.3 Protein Assay 54
4.5.2.4 SDS-PAGE 55
4.5.3 *In vitro* Doxorubicin Release 57
5. CONCLUSIONS AND OUTLOOK 59
5.1 Conclusions 59

5.2 Outlook 63
REFERENCES 64
APPENDIX A. CALIBRATION CURVE FOR PROTEIN ASSAY 73
APPENDIX B. CALIBRATION CURVE FOR DRUG RELEASE 74

LIST OF FIGURES

Figure 2.1	Morphology of NS and NC	4
Figure 2.2	Physico-chemical Properties of Nanocarriers	5
Figure 2.3	Drug Targeting; a) Passive Targeting; b) Active Targeting	7
Figure 2.4	Physiological Environment and Tumor Environment	9
Figure 2.5	Degradation of PLGA to Lactic Acid and Glycolic Acid	11
Figure 2.6	Degradation of PCL	11
Figure 2.7	Effect of PC on Nanocarrier System	12
Figure 2.8	Impact of PC on NPs in the Body	13
Figure 2.9	SPC and HPC Structure	14
Figure 3.1	Miniemulsion-Solvent Evaporation Method	17
Figure 4.1	TEM Images of PLGA NPs at 1 μm scale, (a) PLGA 1, (b) PLGA 2, (c) PLGA 3, (d) PLGA 4, (e) PLGA 5	31
Figure 4.2	SEM Images of PLGA NPs, (a) PLGA 1 at 100 nm scale, (b) PLGA 2 at 100 nm scale, (c) PLGA 4 at 1 μm scale, (d) PLGA 5 at 1 μm scale	31
Figure 4.3	Non-redispersed pellet of PLGA 3	32
Figure 4.4	TEM Images of PCL NPs at 1 μm scale, (a) PCL 1, (b) PCL 2	35
Figure 4.5	SEM Images of PCL NPs at 1 μm scale, (a) PCL 1, (b) PCL 2	35
Figure 4.6	Aggregates of PCL 1 (a) and PCL 2 (b) after Centrifugation at 4 °C, 20.000 g for 1 hour	36
Figure 4.7	Formation of PC Structure on NS Surface	38
Figure 4.8	Silver Stained SDS-PAGE Gels of PC Structure of PLGA 1 NSs, (a) Proteins in FBS PC, (b) Proteins in Human Plasma PC	42
Figure 4.9	Liquid Chromatography-Mass Spectrometry Results, (a) Grouping of Proteins in HPC of PLGA NSs, (b) The Most Abundant Proteins in both Human Plasma and FBS HPC	43
Figure 4.10	Silver Stained SDS-PAGE Gels of PC Structure of PCL 1 NSs, (a) Proteins in FBS PC, (b) Proteins in Human Plasma PC	48

Figure 4.11 Liquid Chromatography-Mass Spectrometry Results, (a) Grouping of Proteins in HPC of PCL NSs, (b) The Most Abundant Proteins in both Human Plasma and FBS HPC 50

Figure 4.12 Silver Stained SDS-PAGE Gels of PC Structure of Dox Encapsulated PLGA 1 NSs, (a) Proteins in FBS PC, (b) Proteins in Human Plasma PC 56

Figure 4.13 *In vitro* Doxorubicin Release from PLGA NSs at 37 °C, pH 7.4 dialysis medium 57

Figure A.1 Calibration Curve of BSA determined from absorbance values at λ=660 nm, measured in millipore H_2O 73

Figure B.1 Calibration Curve of Doxorubicin at pH 7.4 and determined from absorbance values at λ=480 nm 74

LIST OF TABLES

Table 3.1	Specifications of Synthesized PLGA NPs	18
Table 3.2	Specifications of Synthesized PCL NPs	18
Table 3.3	SDS-PAGE Sample Preparation Protocol in the Manufacturer's Instructions	24
Table 4.1	Solid Content of Synthesized PLGA NPs	28
Table 4.2	Size and PDI of Synthesized PLGA NPs	29
Table 4.3	Zeta Potential of PLGA NPs	30
Table 4.4	Size, PDI and Zeta Potential of Centrifuged PLGA NPs	32
Table 4.5	Solid Content of Centrifuged PLGA NPs	33
Table 4.6	Solid Content of Synthesized PCL NPs	34
Table 4.7	Size and PDI of Synthesized PCL NPs	34
Table 4.8	Zeta Potential of PCL NPs	35
Table 4.9	Size, PDI and Zeta Potential of Centrifuged PCL 1	36
Table 4.10	Size, PDI and Zeta Potential of Centrifuged PCL 2	37
Table 4.11	Solid Content of Centrifuged PCL NPs	37
Table 4.12	Size and PDI of PC Coated PLGA 1 NSs	39
Table 4.13	Zeta Potential of PC Coated PLGA 1 NSs	39
Table 4.14	Absorbance and Concentration Values of Proteins in FBS Supernatants of PLGA NSs	40
Table 4.15	Absorbance and Concentration Values of Proteins in Human Plasma Supernatants of PLGA NSs	40
Table 4.16	Size and PDI of PC Coated PCL 1 NSs	45
Table 4.17	Zeta Potential of PC Coated PCL 1 NSs	46
Table 4.18	Absorbance and Concentration Values of Proteins in FBS Supernatants of PCL 1 NSs	46
Table 4.19	Absorbance and Concentration Values of Proteins in Human Plasma Supernatants of PCL 1 NSs	47
Table 4.20	Solid Content of Dox Encapsulated PLGA 1 NSs	51
Table 4.21	Size and PDI of Dox Encapsulated PLGA 1 NSs	51

Table 4.22	Zeta Potential of Dox Encapsulated-PLGA 1 NSs	52
Table 4.23	Encapsulation Efficiency of Dox Encapsulated PLGA 1 NSs	53
Table 4.24	Size and PDI of PC Coated Dox Encapsulated PLGA 1 NSs at pH 7.4	53
Table 4.25	Zeta Potential of PC Coated Dox Encapsulated PLGA 1 NSs at pH 7.4	54
Table 4.26	Absorbance and Concentration Values of Proteins in FBS Supernatants of Dox Encapsulated PLGA 1 NSs	55
Table 4.27	Absorbance and Concentration Values of Proteins in Human Plasma Supernatants of Dox Encapsulated PLGA 1 NSs	55

LIST OF SYMBOLS

%	Percentage
%wt	Weight Percent
°	Degree
°C	Celcius
μg	Microgram
μl	Microliter
g	Relative Centrifugal Force
kDa	Kilodalton
kV	Kilovolt
M	Molar
m^2	Square Meter
mg	Milligram
mL	Milliliter
mM	Millimolar
mV	Millivolt
nm	Nanometer
rpm	Revolution per Minute
v/v	Volume per Volume
w/v	Weight per Volume
ζ	Zeta
λ	Wavelength

LIST OF ABBREVIATIONS

ABC	Ammonium Bicarbonate
BSA	Bovine Serum Albumin
DLS	Dynamic Light Scattering
DOX	Doxorubicin Hydrochloride
ELS	Electrophoretic Light Scattering
EPR	Enhanced Permeability and Retention
FBS	Fetal Bovine Serum
FDA	Food and Drug Administration
H_2O	Water
HER2	Human Epidermal Receptor 2
HPC	Hard Protein Corona
NC	Nanocapsule
NP	Nanoparticle
NS	Nanosphere
PBS	Phosphate Buffered Saline
PC	Protein Corona
PCL	Polycaprolactone
PDI	Polydispersity Index
PGA	Polyglycolic acid
PLA	Polylactic acid
PLGA	Poly(lactide-co-glycolide)
PVA	Poly(vinyl alcohol)
SDS	Sodium Dodecyl Sulfate
SDS-PAGE	Sodium Dodecyl Sulfate Polyacrylamide Gel Electrophoresis
SEM	Scanning Electron Microscopy
SPC	Soft Protein Corona
TEM	Transmission Electron Microscopy

1. INTRODUCTION

1.1 Motivation

Nanomedicine, which focuses on enhancing the therapeutic effect of drugs, is a significant field of biomedical applications. The development of cancer treatment methods that do not harm healthy cells while targeting cancerous cells can be achieved by synthesizing a new nanocarrier system or by improving the properties of the existing system. Biodegradable nanocarrier systems have a crucial role in nanomedicine since they are biocompatible, non-toxic, reduce the toxicity of the encapsulated drugs, and increase the efficiency of treatment by performing controlled and targeted drug release [1, 2].

These systems are exposed to several biomolecules in blood once they are applied to the body intravenously. After the injection of nanocarrier systems into the body, blood proteins adhere to the surface of the nanocarriers within seconds and form the biological fingerprint structure called the protein corona (PC) [3]. Since the fate of the nanocarrier systems under physiological conditions is determined by tightly adhered proteins to the nanocarrier surface in the PC structure, it is essential to obtain detailed knowledge about the PC structure.

As a consequence of all these important points, the motivation of this thesis is to synthesize nanospheres (NSs) and nanocapsules (NCs) using two different biodegradable polymers, PLGA and PCL, and to investigate the PC structure of suitable NP candidates.

1.2 Objectives

The fundamental purpose of this work was to determine the fate of nanocarriers in the body by gaining knowledge on the interactions between nanocarriers and biomolecules. To achieve this aim, the following studies were performed respectively: (i) Biodegradable NSs with polymeric matrix and biodegradable NCs with core-shell structures were synthesized by miniemulsion/solvent evaporation technique using different formulations of PLGA and PCL, respectively. (ii) Their physicochemical and morphological properties were characterized by different characterization methods. (iii) The PC structure was formed around the surface of different NSs selected using human plasma or FBS. (iv) PC coated NSs and proteins formed the PC structure were characterized by various characterization methods. (v) The impact of PC on *in vitro* drug release of PLGA NSs at physiological conditions was investigated.

1.3 Thesis Outline

This thesis consists of five fundamental parts. Chapter 1 explains the motivation, objectives and outline of the thesis. Background information about cancer, nanocarrier systems, polymeric nanocarriers, and protein corona, which are important topics of the thesis, was represented in Chapter 2. Materials and methods used in this study are explained in Chapter 3. The methods are described in five subsections. These subsections are the synthesis of NPs, encapsulation of doxorubicin into NPs, characterization of NPs, characterization of PC structure, and *in vitro* drug release. Chapter 4 includes all experimental results and their discussions. Last, Chapter 5 describes the conclusion and outlook.

2. RESEARCH BACKGROUND

2.1 Cancer

Cancer, one of the most prevalent illnesses, is seen as 19.3 million new cases and caused 10 million deaths in 2020 [4]. In the United States, it was expected 1.918.030 new cancer cases and 609.360 deaths in 2022 according to previous statistics [5]. It refers to the formation of regional abnormal tissue masses due to the abnormal proliferation of cells by random division [6]. Each conventional treatment methods for cancer, which are surgery, chemotherapy, radiotherapy and immunotherapy, have its own limitations and disadvantages. While surgery is an effective method in the early stage, it may not be sufficient in the late stage. In addition, surgery carries risks depending on the area where the abnormal tissue is located. Chemotherapy causes the death of all growing cells without distinguishing between cancer cells and healthy cells since it is based on non-targeted chemotherapeutic drug treatment. While this causes many side effects such as hair loss and bone marrow suppression, it also has limitations as a consequence of its poor solubility and short half-life. Radiation aims to reduce the size of abnormal tissue by using high-energy rays such as X-rays. While it is tried to achieve this goal, high-energy rays can also damage healthy tissue around the abnormal tissue [4, 7, 8]. All these limitations and disadvantages led to the need for a new treatment method that is more effective, safer and reduces the side effects.

2.2 Nanocarrier Systems

Nanomedicine, which refers to the development of nanoscale materials to improve healthcare and provide new solutions for human health, is a significant technology for diagnosis, imaging, therapies, tissue engineering, and drug delivery systems [9, 10]. Chemotherapeutic drug loaded nanocarrier systems are a type of treatment used to increase drug stabilization, reduce the toxicity of drugs, and perform the controlled re-

lease of drugs. Moreover, these colloidal systems are promising drug delivery systems since they enhance biodistribution and pharmacokinetics [11]. By surface modification, these nanocarrier systems are able to target directly specific cells, cancerous cells in this case. When they reach cancerous cells, they release their cargo and kill the abnormal cells. In this way, these systems improve the solubility problem of chemotherapeutic agents by encapsulating them whereas targeting therapy prevents chemotherapeutic agents from causing cytotoxic effects in healthy cells, reducing side effects [12].

Polymeric nanocarriers, which can be classified as nanospheres or nanocapsules according to their morphology, have diameters between 1 to 100 nanometers. While nanospheres contain only a polymeric network, nanocapsules have a shell structure and a core structure consisting of an oil phase [13]. In NSs, the drug shows a homogeneous distribution in the polymer network. However, the drug is encapsulated in the inner core consisting of the oil phase in NCs [14].

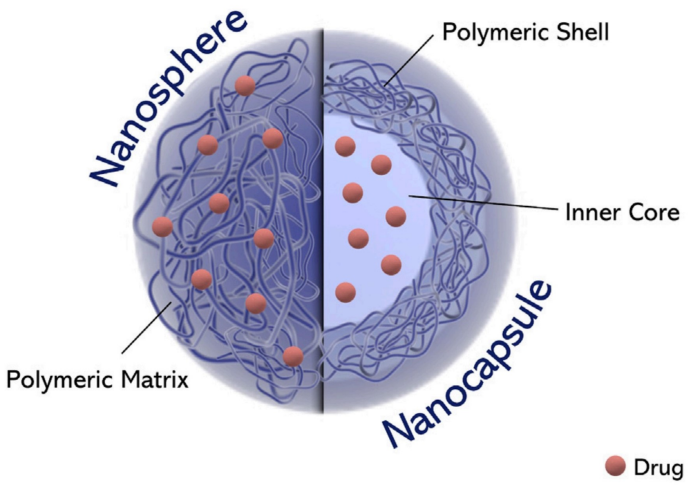

Figure 2.1: Morphology of NS and NC [14]

2.2.1 Physico-chemical Properties of Nanocarriers

The size, shape, and surface characteristics of nanocarriers, which are physico-chemical properties, have a substantial influence on drug release and their circumstance in the bloodstream [14].

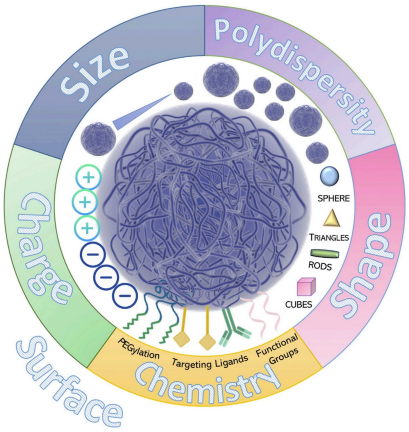

Figure 2.2: Physico-chemical Properties of Nanocarriers [14]

2.2.1.1 Size

Drug loading effectiveness and capacity, *in vivo* stability, targeting potential, and biological fate of these systems are all influenced by particle size and size distribution. Since the surface area-to-volume ratio is higher in smaller nanocarriers, the chemotherapeutic agents will be near or at the surface of particles, causing quicker drug release. On the other hand, larger nanocarriers exhibit slower drug release and have more encapsulated agents due to their larger cores. Nanocarriers with a diameter of less than 10 nm can be quickly filtered and removed from the body by the kidneys [8, 15].

2.2.1.2 Shape

The biodistribution, blood circulation, and cellular uptake of nanocarriers are all significantly influenced by their shape. They can be produced as spherical, filamentous, or tubular. This has a substantial role in active targeting, as the area of contact with

the receptors on the cell membrane will alter depending on their shape. For instance, the increased contact area of rod nanocarriers results in a more effective cell interaction when compared to spherical nanocarriers. But it was found that spherical nanocarriers were less toxic [16, 17].

2.2.1.3 Surface Properties

When surface properties are discussed, the most important considerations are surface charge, hydrophobicity/hydrophilicity, and surface modification.

Zeta potential indicates the charge of nanocarriers at the slipping plane and has an important role in understanding their toxicity in the bloodstream. Nanocarriers can be anionic, cationic or neutral. Cationic nanocarriers can be attracted to the cellular membrane as the cell membrane is negatively charged. However, it was discovered that cationic nanocarriers have a more toxic effect on cells than anionic nanocarriers. Nanocarriers interact with plasma proteins and surface charge influences the variety of absorbed proteins to the surface. As a result of the absorbed proteins, either the mononuclear phagocyte system removes the nanocarriers from the circulation or their circulation time is increased [14, 17].

Surface modification determines the stability of nanocarriers and their success in active transport. Overexpressed receptors on the cancer cells are targeted by binding the specific ligands of these receptors on the nanocarriers' surface. Thereby, cellular uptake of surface-modified nanocarriers is increased by active targeting [16].

2.2.2 Drug Targeting

Drug delivery of drug-loaded nanocarriers is as important as the synthesis of biocompatible and biodegradable nanocarriers. The drug systems must be delivered to the cancerous cells after the chemotherapeutic agents are encapsulated inside the

nanocarriers. There are two ways to carry out this delivery, active targeting or passive targeting [18].

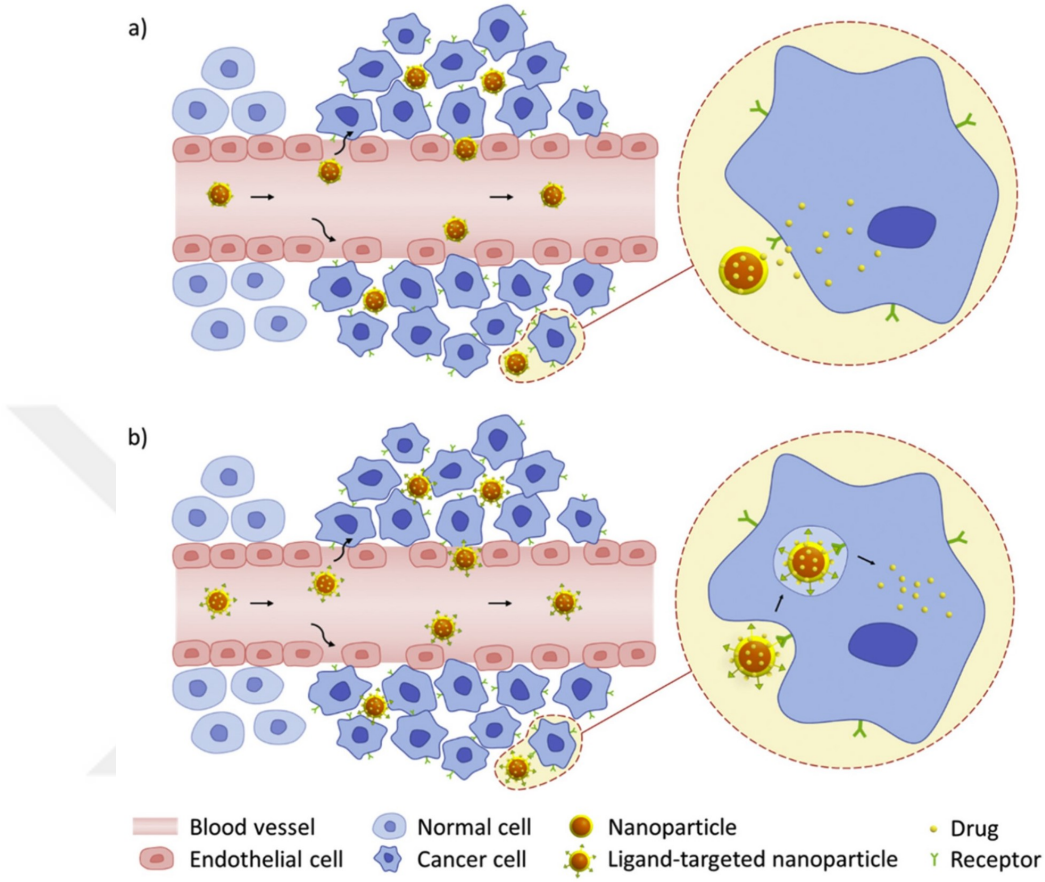

Figure 2.3: Drug Targeting; a) Passive Targeting; b) Active Targeting [7]

2.2.2.1 Active Targeting

Specific receptors being overexpressed more in cancer cells than in healthy cells underlies the active targeting. Surface modifications occur by binding ligands specific to these receptors to the surfaces of nanocarriers; therefore, these nanocarriers directly target cancerous cells. Nanocarriers are internalized by receptor-mediated endocytosis thanks to the interaction between receptors on the cancerous cells' surface and ligands attached to the nanocarriers' surface [8]. The receptor-ligand strategy enables increased affinity of nanocarriers to cancer cells, leading to enhancement of drug penetration [19].

A significant illustration of a receptor that is overexpressed on cancer cells is transferrin. It has been observed that it is overexpressed 100 times more in cancer cells. Folate receptor, another significantly overexpressed receptor, has a crucial role in nucleotide synthesis during the uncontrolled rapid division of cancer cells. Folic acid-conjugated nanocarriers perform direct binding to folate receptors. Epidermal receptor 2 (HER2) and epidermal growth factor receptor (EGFR) are two important overexpressed receptors in breast cancer [20].

2.2.2.2 Passive Targeting

Passive targeting is based on the accumulation of nanocarriers in the tumor tissues due to the abnormalities of the tumor vasculature. Physico-chemical properties of nanocarriers determine whether nanocarriers will accumulate in tumor tissue or will be removed by mononuclear phagocyte system [21, 22]. The accumulation of nanocarriers in tumor tissue resulting from tumor vasculature is explained by enhanced permeability and retention effect (EPR). Enhanced retention and enhanced permeability are the two main parts of the EPR effect [23].

Solid tumor cells begin to form their own vascular when they are between 150 and 200 nm in size, which triggers the angiogenesis process. As the tumor size increases, the tumors will constrict the blood vasculature and reduce blood flow, causing the production of angiogenic factors that cause angiogenesis. Newly formed blood vessels have a different structure due to large gaps caused by abnormal irregular and discontinuous endothelial structure, loose attachment to pericyte endothelial cells, or lack thereof. These abnormalities give rise to the formation of large fenestrations providing enhanced permeation which nanocarriers can pass through these windows and accumulate in tumor tissue [23].

In healthy tissues, extra fluid is continuously drained into the lymphatic system to keep interstitial fluid balance. However, tumor tissues lack lymphatic drainage. Lymphatic vessels which are functional are only present in the lymphatics of nearby

healthy tissues. This situation ensures the retention of nanocarriers in tumor tissues [20].

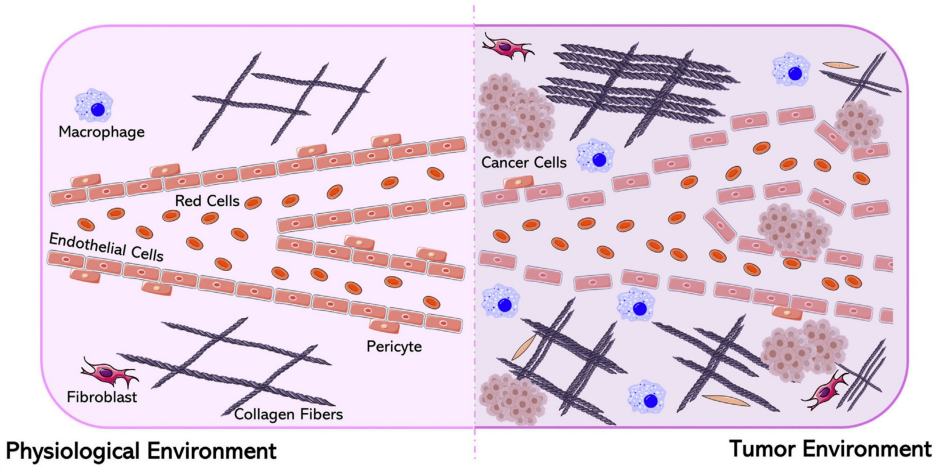

Figure 2.4: Physiological Environment and Tumor Environment [14]

2.3 Polymeric Nanocarriers

Polymers, one of the most important examples of biomaterials, are divided into two categories as natural and synthetic polymers. Although natural polymers containing polysaccharides and proteins are biocompatible and biodegradable, they have disadvantages because of uncontrolled physicochemical properties and manufacturing, tending to microbial contamination, and variation from batch to batch [24–26]. On the other hand, synthetic polymers have important advantages owing to the adjustability of their molecular weight and crystallinity, the controllability of their synthesis, and the predictability of their physicochemical properties [27].

Cellulose, starch, chitosan, alginate, and hyaluronic acid constitute polysaccharides, while collagen, gelatin, silk, and albumin are protein-based polymers that are often used [28]. Nonetheless, synthetic polymers are divided into biodegradable and non-biodegradable polymers. Polyester, poly(ortho ester), polyamide, polyanhydride, and phosphorus-based polymers can be given as examples of synthetic polymers used for drug release due to their biodegradability properties. PLGA and PCL are two important biodegradable polyesters and are often used as drug delivery systems because

of their properties [29].

2.3.1 Poly(lactic-co-glycolic acid) (PLGA)

PLGA is the FDA-approval biodegradable polymer obtained by copolymerization of polylactic acid (PLA) and polyglycolic acid (PGA). The molecular weight, degradation rate, and crystallinity of PLGA are able to be changed by adjusting the ratio of hydrophobic PLA to hydrophilic PGA. For instance, the higher the amount of glycolic acid in the structure, the faster the degradation [24, 30]. Conversely, the copolymer of lactic acid:glycolic acid (50:50) is the type of PLGA with the fastest degradation [31]. Hydrolysis of ester bonds found in the structure performs the degradation of PLGA into two non-toxic monomers, lactic acid and glycolic acid, which participate in biochemical pathways in the body, by bulk erosion [32].

PLA has three isomers, $_{L}$-PLA, $_{D}$-PLA, and $_{D,L}$-PLA. $_{D,L}$-PLA is more used PLA type in biomedical applications since its biocompatibility is excellent and its molecular weight is lower. Moreover, it has better stability than other types of PLA [33]. PLGA is a valuable polymer for NP synthesis because of its high biodegradability and ability of high encapsulation efficiency. For instance, Chittasupho et al. encapsulated doxorubicin hydrochloride into PLGA NPs with 75% drug encapsulation [34]. In addition, BIND Therapeutics company works to develop a treatment against prostate cancer by targeting prostate-specific membrane antigen via encapsulating docetaxel into PEG-PLGA NPs that are in the process of human testing [35, 36].

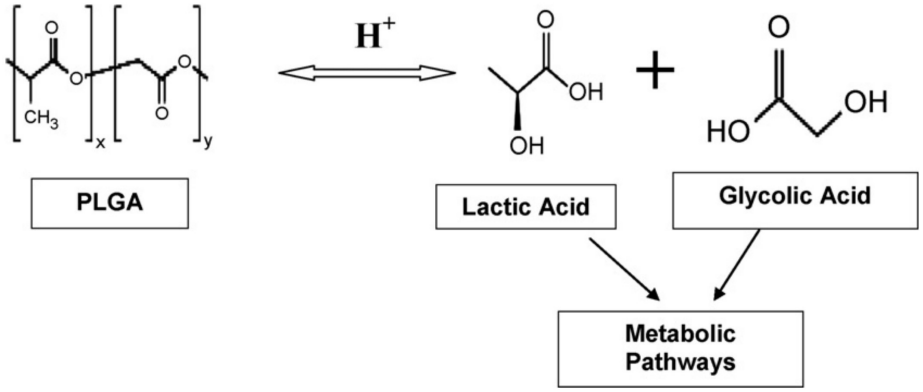

Figure 2.5: Degradation of PLGA to Lactic Acid and Glycolic Acid [32]

2.3.2 Polycaprolactone (PCL)

PCL is a hydrophobic, semicrystalline polyester obtained by ring-opening polymerization of ϵ-caprolactone by enzymes. Its melting point is 60 °C while its glass transition point is -60 °C. The hydrolysis of ester bonds in its structure degrades the PCL to 6-hydroxycaproic acid, which then participates in the citric acid cycle and is completely metabolized [30, 37]. PCL is a good candidate for long-term drug delivery as its degradation is slower compared to PLGA. Furthermore, it is a suitable synthetic polymer for biomedical applications because of its biocompatibility and rapid cellular uptake via endocytosis [38].

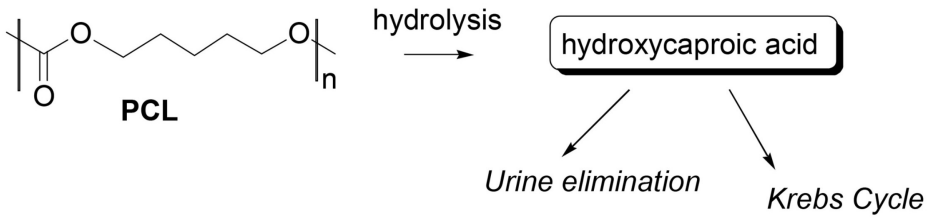

Figure 2.6: Degradation of PCL [39]

2.4 Protein Corona

NPs encounter biological barriers when they are injected into the body intravenously. One of these important barriers is plasma proteins in the blood. Plasma proteins bind tightly or slightly to the surface of NPs, forming a layer called the PC [40].

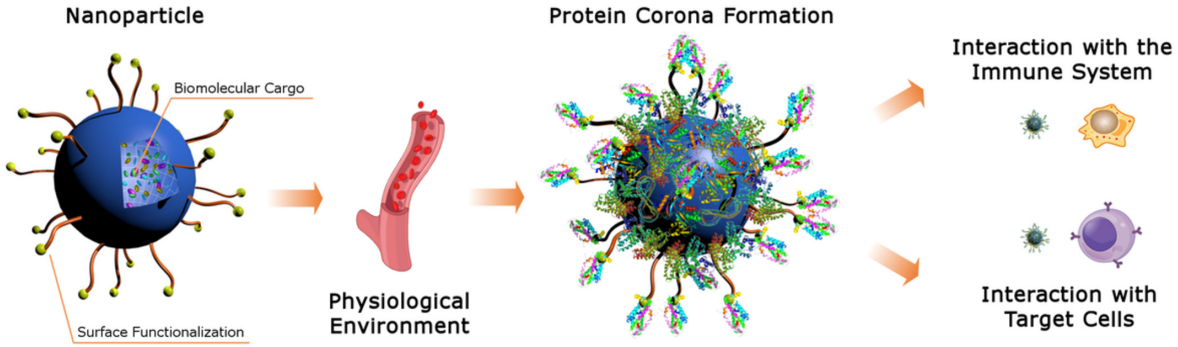

Figure 2.7: Effect of PC on Nanocarrier System [41]

Although NPs have been characterized *in vitro* in terms of hydrodynamic size, zeta potential or drug release, these characterizations alter when they are injected into the physiological environment [42]. The PC formed by the proteins adhering to the NP surface affects the duration in the bloodstream of NPs, their cellular uptake, penetration into the tumor tissue and accumulation there. Therefore, knowing which proteins make up the PC structure helps to understand the fate of these NPs in the body [43, 44].

PC is able to affect the physiological conditions of NPs positively as well as negatively. If there are more proteins called opsonin in the PC structure, these proteins stimulate the mononuclear phagocyte system, and the NPs are captured by the mononuclear phagocytic system, followed by removal from the body [45]. However, if this structure is mostly composed of dysopsonins, the NPs gain a stealth property, and their blood circulation time is prolonged. If the NPs' surface is modified with a specific ligand, the formation of a PC on the surface might also have a negative result on the cellular uptake of the NPs as it will reduce the interaction of these modified NPs with the cell membrane. Conversely, some proteins that form the PC may enhance the internalization of NPs as they may be specific to the overexpressed receptors in cancer

cells [46]. For all these reasons, it is crucial to know which proteins are found in the PC structure.

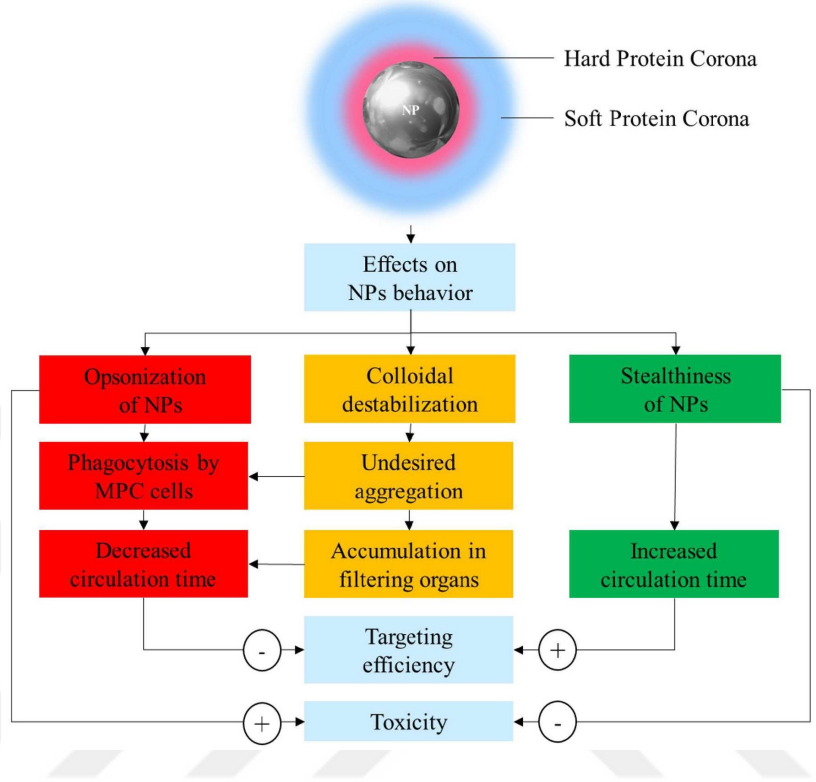

Figure 2.8: Impact of PC on NPs in the Body [47]

2.4.1 Structure of Protein Corona

The PC structure is classified into SPC and HPC. Proteins in SPC bind either to the NPs' surface weakly or to the other proteins via protein-protein interaction. They are located in the outer layer of the PC due to slight interaction. Therefore, the binding of proteins can be easily disrupted and they can be replaced by other proteins in the biological environment [48].

On the other hand, the proteins in the HPC adhere directly to the NP surface and their replacement with the new proteins is very slow. These proteins form the inner layer of the PC structure as they have a high affinity to the NP surface [49, 50].

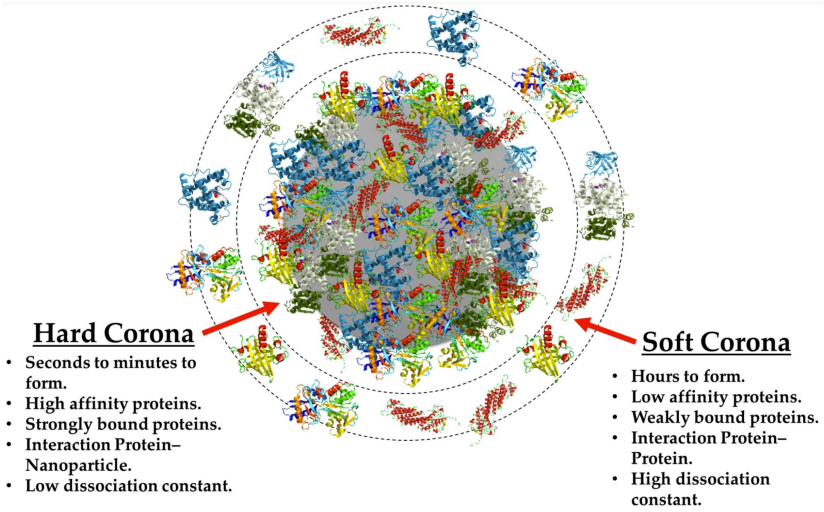

Figure 2.9: SPC and HPC Structure [51]

2.4.2 Types of Proteins in Protein Corona

Proteins in the PC structure are classified as opsonin and dysopsonin. Opsonins cause the removal of NPs from blood circulation by stimulating the mononuclear phagocyte system. In this case, the NPs are cleared before they reach the target cell. Conversely, proteins called dysopsonins provide NPs the stealth property, preventing their uptake by macrophages, and allowing them to stay in the blood circulation longer [52]. Immunoglobulins, complements and fibrinogen are the main opsonins, whereas serum albumin, transferrin and apolipoproteins are significant dysopsonins [40, 53, 54].

2.4.3 Characterization of Protein Corona

After the formation of PC, PC coated NPs can be characterized in respect of size, surface charge, PC composition, binding capacity and PC conformation [48].

Dynamic light scattering (DLS) is a frequently used method to detect the change in the size of PC-coated and non-coated NPs. Its size is measured in relation to Brownian motion, which is defined as the random motion of NPs in dispersion due to the bombardment of surrounding molecules. By determining their diffusion coefficient

under Brownian motion, their hydrodynamic size is calculated using Stokes-Einstein equation [55, 56].

The change in surface charge of PC coated NPs is studied by electrophoretic light scattering (ELS) method. It was found that the surface charge of most PC-coated NPs is negative at physiological conditions [48].

Each PC structure is unique to NPs. Thus, identification of the protein composition is significant to understand the NP's fate in the physiological environment. The protein composition in the PC structure can be identified by SDS-PAGE or mass spectrometry [56]. In SDS-PAGE, an electric field is applied to protein samples to separate them according to their molecular weight. However, if there are proteins with similar molecular weights, they cannot be detected separately [57]. Mass spectrometry is an effective method for the determination of individual proteins in HPC. Thus, by detecting the proteins with the highest concentration around the NPs, it can be understood whether the NPs are more likely to be captured by immune system cells or are more likely to gain stealth properties [48, 58].

3. METHODS

3.1 Materials

Poly(D,L-lactide-co-glycolide) (PLGA) (Resomer RG 505, molecular weight 54.000-69.000), poly(vinyl alcohol) (PVA) (Molecular weight 9.000-10.000, 80% hydrolyzed), polycaprolactone (PCL) (Mn 45.000), olive oil (highly refined, low acidity), ethyl acetate (ACS reagent, ≥99.5%), sodium dodecyl sulfate (SDS) (ACS reagent, ≥99.0%), hydrochloric acid (ACS reagent, 37%), sodium phosphate dibasic heptahydrate (ACS reagent, 98.0-102.0%), sodium phosphate monobasic monohydrate (ACS reagent, ≥98%), bovine serum albumin (BSA) (heat shock fraction, protease free, fatty acid free, essentially globulin free, pH 7, ≥98%), trizma® hydrochloride solution (1 M, BioReagent, for molecular biology), dulbecco′s phosphate buffered saline (PBS) (modified, without calcium chloride and magnesium chloride, liquid, sterile-filtered, suitable for cell culture), ProteoExtract® Protein Precipitation Kit (Cat 539180), DL-Dithiothreitol (BioUltra, for molecular biology, ≥99.5% (RT)) and iodoacetamide (BioUltra) were supplied by Sigma Aldrich.

Chloroform (ACS Grade, ≥ 99.8%), acetic acid (Glacial, ACS Grade, ≥ 99.7%) and potassium chloride (Reagent Grade, >=99%) were bought from Fisher Scientific.

Ethanol (Absolute, Reag. ISO, Reag. Ph. Eur., liquid (clear, colorless), ≥99.8% (GC)) and ammonium bicarbonate (Eluent additive for LC-MS) were bought from Honeywell.

Doxorubicin HCl was supplied by Biosynth Carbosynth. Dialysis membrane (MWCO 6000-8000) was bought from Carl Roth.

Fetal Bovine Serum (FBS) (qualified, Brazil) was purchased from Gibco. Pierce™ 660nm protein assay reagent, ionic detergent compatibility reagent for Pierce™ 660nm protein assay reagent and low protein binding microcentrifuge tubes (2 mL), Pierce™ detergent removal spin columns were supplied from Thermo Scientific.

4X Bolt™ LDS Sample Buffer, 10X Bolt™ Sample Reducing Agent, Bolt™ 10%, Bis-Tris, 1.0 mm, Mini Protein Gels, 20X Bolt™ MES SDS Running Buffer, Simply-

Blue™ SafeStain, SeeBlue™ Plus2 Pre-stained Protein Standard and SilverQuest™ Silver Staining Kit were bought from Invitrogen™. Sequencing grade modified trypsin (V5111) was bought from Promega. RapiGest SF surfactant was supplied by RapiGest. Ampuwa was bought from Fresenius Kabi Deutschland GmbH. Acetonitrile (ULC/MS - CC/SFC) and Water (ULC/MS - CC/SFC) were supplied by Biosolve Chimie SARL.

3.2 Methods

3.2.1 Synthesis of Nanoparticles

Two sorts of nanoparticle morphology were studied: Nanospheres (NSs) and Nanocapsules (NCs) were synthesized by direct miniemulsion-solvent evaporation method (Figure 3.1).

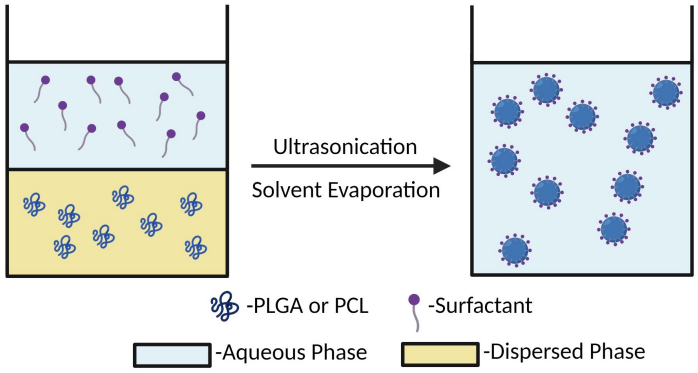

Figure 3.1: Miniemulsion-Solvent Evaporation Method.

The phase called dispersed phase was obtained by dissolving polymers (PLGA or PCL) in organic solvent while the surfactant was dissolved in millipore H_2O to acquire the aqueous phase. Unlike the NS synthesis, a certain amount of olive oil was added to the dispersed phase to form the core structure in the NC synthesis by modifying as follows [59]. Then, the dispersed phase was added to the aqueous phase. Solution was stirred at 1000 rpm for 1 hour at 25 °C to obtain macroemulsion. Subsequently, ultrasonication was performed under an ice bath for 2 minutes at 70% amplitude for 10 second sonication and 10 second pulse using Branson 450W Sonifier. The organic

solvent was evaporated at room temperature by stirring the dispersion at 300 rpm for 16 hours. The filtration of dispersion was carried out slowly using Kimtech wipes [60]. Detailed information about the amount of material used and the type of organic solvent is given in Table 3.1 and Table 3.2.

Table 3.1: Specifications of Synthesized PLGA NPs

Sample		Surfactant		Lipid		Organic Solvent	
Type	Amount (mg)	Type	Amount (mg)	Type	Amount (mg)	Type	Amount (mL)
PLGA 1	100	PVA	150	-	-	Chloroform	2.5
PLGA 2	100	PVA	150	-	-	Ethyl acetate	2.5
PLGA 3	150	SDS	10	Olive oil	300	Chloroform	1.8
PLGA 4	150	PVA	225	Olive oil	300	Chloroform	1.8
PLGA 5	100	PVA	150	Olive oil	200	Chloroform	1.8

Table 3.2: Specifications of Synthesized PCL NPs

Sample		Surfactant		Lipid		Organic Solvent	
Type	Amount (mg)	Type	Amount (mg)	Type	Amount (mg)	Type	Amount (mL)
PCL 1	100	PVA	150	-	-	Chloroform	2.5
PCL 2	100	PVA	150	Olive oil	300	Chloroform	1.8

3.2.2 Encapsulation of Doxorubicin into Nanoparticles

10 mg Doxorubicin HCl (Dox) and 100 mg PLGA were added into 2.5 mL chloroform and stirred until obtaining a completely dissolved solution. Drug included solution was added into the aqueous phase containing 150 mg PVA dissolved in 10 mL millipore H_2O [61]. Macroemulsion formation and NS synthesis took place as described in Section 3.2.1.

3.2.3 Characterization of Nanoparticles

Synthesized NSs and NCs were characterized regarding their solid content, size, polydispersity index (PDI), zeta potential, morphology, centrifugation stability and encapsulation efficiency.

3.2.3.1 Solid Content Analysis

Solid content was analyzed for each sample as triplicates by modifying from Iyisan et al. (2020) [59]. First, empty 2 mL eppendorfs were weighed. Then, 100 μL from each sample was poured into the eppendorfs and filled eppendorfs were weighted. The weights of the 100 μL samples were calculated by subtracting the weight of the filled eppendorfs from the weight of the empty eppendorfs. Each sample was frozen using liquid nitrogen and kept in the Christ Alpha 2-4 LD plus freeze-dryer instrument for 16 hours to dry. After freeze-drying, each eppendorf was weighed and weights of dried 100 μL samples were calculated.

3.2.3.2 Size and Polydispersity Index Measurement

Size and PDI were analyzed by Dynamic Light Scattering (DLS) (Zetasizer Nano S90, Malvern Instruments, U.K.). All samples were diluted in millipore H_2O. Then, measurements were carried out in triplicate at an angle of 90° and 25 °C [62].

3.2.3.3 Zeta Potential Analysis

Zeta (ζ) potential measurements were carried out by Electrophoretic Light Scattering (Malvern Zetasizer Nano Z, Malvern Instruments, U.K.). 50 μL of samples were diluted in 1 mL of 1 mM Potassium Chloride solution at 25 °C. Measurements were performed in triplicate [62].

3.2.3.4 Morphological Characterization

Morphology of synthesized NSs and NCs was characterized by transmission electron microscopy (TEM) and scanning electron microscopy (SEM).

In *TEM* preparation, NSs and NCs were diluted, followed by dropping onto the 300-mesh carbon-coated copper grids. Imaging was performed using JEOL 1400 Transmission Electron Microscope (Jeol Ltd., Tokyo, Japan) at 120 kV acceleration voltage [62].

For *SEM*, NSs and NCs were diluted, then dropped onto a silicon wafer and dried at room temperature. Imaging was carried out using Gemini 1530 (Carl Zeiss AG Oberkochem, Germany) at 0.35 kV [62].

3.2.3.5 Centrifugation

All samples were centrifuged to determine the formation of pellet and redispersion conditions before starting the Protein Corona (PC) experiment. PLGA NSs and NCs were centrifuged three times at 4 °C, 20.000 g for 1 hour [63]. PCL NSs and NCs were centrifuged three times at 4 °C, 15.000 g for 30 minutes [64].

After centrifugation, solid content analysis of the centrifuged samples was performed as specified in Section 3.2.3.1 to determine the loss during centrifugation. 400 μL sample was weighed instead of 100 μL due to the possible loss.

3.2.3.6 Determination of Encapsulation Efficiency

During PC experiments, 4 mL of supernatants of human plasma coated Dox encapsulated NSs, FBS coated Dox encapsulated NSs, or NSs in the control group were collected after each centrifugation at 4 °C, 20.000 g for 1 hour. Their absorbance val-

ues at 480 nm were measured by Infinite M1000 microplate reader instrument (Tecan, USA). The concentrations corresponding to their absorbance values were calculated using the previously prepared Dox calibration curve (Figure B.1). Free Dox amount in all supernatants was summed up. Subsequently, the total free Dox amount was subtracted from the initial Dox amount which was 10 mg, and the amount of encapsulated Dox was obtained [65]. The encapsulation efficiency was calculated using Equation 3.1 below.

$$Encapsulation\ Efficiency = \frac{Initial\ Dox\ amount - Free\ Dox\ amount}{Initial\ Dox\ amount} x100 \quad (3.1)$$

3.2.4 Protein Corona Formation

Before PC formation around the surface of NSs, the necessary volume for 0.05 m^2 surface area of NSs was calculated. The required volume corresponding to 0.05 m^2 surface area was calculated according to Equation 3.2. The weight of a NS (m_{dryNS}) was determined by multiplying its volume and density after the volume of a NS was calculated using the radius obtained by DLS. The total number of NSs in the 0.05 m^2 surface area (N_{NS}) was calculated by dividing the 0.05 m^2 surface area by one NS area. Then, the total weight of NSs in the 0.05 m^2 surface area was determined by multiplying the weight of one NS by the total number of NSs in the 0.05 m^2 surface area. The required NS volume, corresponding to a surface area of 0.05 m^2, was calculated by dividing the total weight by the solid content [66].

$$V_{dispersion\ of\ 0.05\ m^2\ NSs} = \frac{(N_{NS})(m_{dryNS})}{solid\ content} \quad (3.2)$$

Subsequently, PC was formed around the surface of NSs by using either human plasma or FBS. Pooled human blood plasma was stored at -20 °C until use. 15 mL of frozen human plasma was thawed and aliquots were prepared in 2 mL Thermo Scientific™ Low Protein Binding Microcentrifuge Tubes. Human plasma was span

down at 4 °C, 15.000 g for 30 minutes to remove aggregated proteins before use. The transfer of supernatant was done to a new tube. The amount of human plasma to be used was kept at 4 °C while the rest was stored at -20 °C. 50 mL of FBS (Gibco™ 10270, qualified, Brazil) was divided into 3 mL aliquots and stored at -20 °C until use.

PLGA 1 was used to investigate the interaction between proteins and NSs. 142.2 μL of PLGA 1 was incubated with either 1 mL human plasma or 1 mL FBS at 37 °C, 300 rpm for 1 hour. After incubation, they were centrifuged at 4 °C, 20.000 g for 1 hour to remove unbound proteins. The supernatants were collected as "FBS Soft PC or Human Plasma Soft PC". Pellets were redispersed in 1 mL PBS to wash and centrifuged three times at 4 °C, 20.000 g for 1 hour. The supernatants were collected at each step, respectively named as "Wash 1, Wash 2 and Wash 3". After the last centrifugation, pellets were redispersed in 100 μL of 2% (w/v) SDS (62.5 mM Tris*HCl) desorption buffer, followed by incubation at 95 °C, 300 rpm for 5 minutes to break down the bonds between proteins found in the HPC and surface of NSs. Redispersions were centrifuged at 4 °C, 20.000 g for 1 hour. Supernatants, which were named as "Hard PC", were transferred to a fresh 2 mL Thermo Scientific™ Low Protein Binding Microcentrifuge Tubes to perform protein quantification, SDS-PAGE and liquid chromatography-mass spectrometry [63].

The same protocol and amounts were applied to Dox encapsulated PLGA NSs to form the PC layer around the NSs. After the last washing centrifugation, some pellet of Dox encapsulated PLGA 1 was redispersed in 0.01 M pH 7.4 sodium phosphate buffer. On the other hand, some pellet was redispersed in a desorption buffer. All supernatants were stored for protein quantification, SDS-PAGE and encapsulation efficiency.

PCL 1 was used to analyze the interaction between proteins and NSs. 107.86 μL of PCL 1 was used to form the PC structure. In this protocol, PCL NSs were centrifuged at 4 °C, 15.000 g for 20 minutes after incubation with either 1 mL human plasma or 1 mL FBS at 37 °C, 300 rpm for 1 hour. The centrifugation conditions during washing were also maintained in this condition. After the third washing and redispersion of the pellet in 100 μL desorption buffer, they were centrifuged at 4 °C,

20.000 g for 1 hour. All supernatants were stored in 2 mL Thermo Scientific™ Low Protein Binding Microcentrifuge Tubes for protein analysis [63].

3.2.5 Analysis of Protein Corona Structure

3.2.5.1 Protein Assay

The calibration curve of Bovine Serum Albumin (BSA) was prepared to determine the concentration of obtained proteins after each centrifugation. 2 mg/mL BSA stock solution was prepared by dissolving it in millipore H_2O and then, BSA dilution series were obtained in the range of 31.25 and 2000 μg/mL. 10 μL of each BSA standard was added into 96 well-plates as triplicates. Then, 150 μL of Thermo Scientific Pierce 660 nm Protein Assay Reagent was added into each wells containing BSA standards. The 96 well-plate was shaken orbitally for 60 seconds, followed by measurement of absorbance values of BSA standards at 660 nm by a microplate reader using Tecan Infinite M1000 Instrument (Tecan, USA). 10 μL of the proteins obtained after each centrifugation and have unknown concentrations, respectively Soft PC, Wash 1, Wash 2, Wash 3, and Hard PC, 10 μL of FBS, 10 μL of human plasma and 10 μL of millipore H_2O were added to 96 well-plates as triplicates. 150 μL of Thermo Scientific Pierce 660 nm Protein Assay Reagent containing Thermo Scientific Pierce Ionic Detergent Compatibility Reagent was added into each well. After orbitally shaking for 60 seconds, absorbance of samples at 660 nm was measured by Infinite M1000 microplate reader (Tecan, USA). Millipore H_2O was used as blank during the measurement. Concentrations of protein samples were determined by utilizing the BSA calibration curve (Figure A.1) [67].

3.2.5.2 SDS-PAGE

The specific protein concentrations that were loaded into the gel were identified for each sample based on the concentrations obtained from the protein assay. SDS-

PAGE samples were prepared depending on the sample preparation protocol in the manufacturer's instructions (Table 3.3). After the samples were prepared according to the protocol, they were incubated at 70 °C, 300 rpm for 10 minutes and then loaded into the wells. 10 μL of SeeBlue™ Plus2 Pre-stained Protein Standard was loaded into the first well. The gel was run for 1 hour at constant 100 volts. The gel was stained with a silver staining kit at the end of the run [68].

Table 3.3: SDS-PAGE Sample Preparation Protocol in the Manufacturer's Instructions

Materials	Amount (μL)
Sample	x
4X Bolt LDS Sample Buffer	2.5
10X Bolt Reducing Agent	1
Water	up to 6.5
Total	10

3.2.5.3 Silver Staining

SilverQuest Silver Staining Kit was used according to the manufacturer's instructions. The gel was washed with ultrapure water, then fixed with 50 mL fixative solution containing 25 mL Ampuwa sterile water, 20 mL ethanol and 5 mL acetic acid for 20 minutes. Subsequently, the gel was washed in 50 mL of 30% ethanol for 10 minutes. Ethanol solution was removed, and gel was incubated with 50 mL sensitizing solution containing 30 mL sterile water, 15 mL ethanol and 5 mL sensitizer for 10 minutes. Gel was washed with 50 mL 30% ethanol and 50 mL sterile water for 10 minutes, respectively. 50 mL staining solution containing 49.5 mL sterile water and 0.5 mL stainer was added to the gel, followed by incubation for 15 minutes. Then, gel was washed with 50 mL sterile water for 20-60 seconds. Gel was incubated with 50 mL developing solution containing 45 mL sterile water, 5 mL developer and 1 drop developer enhancer for 4-8 minutes until bands appeared. When bands appeared, 5 mL stopper was added to the gel, followed by incubation for 10 minutes [68]. The gel was then washed with 50 mL of sterile water and imaged by View Pix 1100 (Epson, Japan).

3.2.5.4 Protein Digestion in Solution

Pierce Detergent Removal Spin Columns was used to remove SDS before protein digestion. The addition of 100 μL sample in the column was performed and the column was placed in a LoBind tube, followed by centrifugation at 1500 g for 2 minutes. Proteins were digested according to the manufacturer's instructions. They were precipitated using ProteoExtract Protein Precipitation Kit. After they were centrifuged at 10.000 g for 2 minutes and washed in the wash solution, the pellet was dried for 2 minutes. 100 mg RapiGest SF was dissolved in 1 mL 50 mM ammonium bicarbonate (ABC) buffer. Pellet was redispersed in ABC buffer and incubated at 300 rpm, 80 °C for 15 minutes. 5 μL of 100 mM dithiothreitol was added, and incubation was performed at 300 rpm, 56 °C for 45 minutes. When the sample temperature reached room temperature, 3 μL of 500 mM iodoacetamide was added and they were incubated for 1 hour in the dark at room temperature. Protein digestion was carried out by adding 3 μL of trypsin to the 15 μg protein sample. This incubation was performed at 300 rpm, 37 °C for 16 hours. The digestion reaction was stopped by incubation of the sample with 2 μL hydrochloric acid at 37 °C for 45 minutes. The sample was centrifuged at 13.000 g for 15 minutes and the supernatant was collected [69].

3.2.5.5 Liquid Chromatography-Mass Spectrometry

20 μL sample was diluted in 18 μL LC-MS water containing 0.1% formic acid followed by 2 μL Hi3 *Escherichia coli* standard addition. Peptides were separated using a nanoACQUITY UPLC system consisting of a C18 analytic reversed-phase column (1.7 mm, 75 mm x 150 mm, Waters, USA) and a C18 nanoACQUITY Trap Column (5 mm, 180 mm x 20 mm). 0.1% (v/v) formic acid in water (A) and 0.1% (v/v) formic acid in acetonitrile (B) were prepared as the mobile phases. Over the course of 90 minutes, the separation was carried out using a gradient of 5% to 40% of mobile phase B. The Synapt G2- Si mass spectrometer and the nanoACQUITY UPLC system were coupled. The flow rate of the sample was adjusted to 0.3 μL/min, and the flow rate of Glu-Fibrinopeptide and Leu-Enkephalin used as reference was arranged to 0.5

μL/min. Using a NanoLockSpray source, electrospray ionization was performed in positive ion mode. Progenesis QI was used for the analysis of protein identification using a human database constituted by Uniprot. The database included the peptide sequence of the Hi3 *E. coli* standard and the approach of TOP3/Hi3 was used for protein quantification [67, 70].

3.2.6 *In vitro* Release of Doxorubicin

First, a Dox calibration curve was prepared at pH 7.4. Then, drug release experiment at this pH value was performed.

3.2.6.1 Doxorubicin Calibration Curve

Dox samples in the range of 5-55 μg/mL were prepared by dissolving 1 mg Dox in 20 mL 0.01 M pH 7.4 sodium phosphate buffer. 150 μL of each dilution was added into 96-well plates as triplicates and measurement of their absorbance at 480 nm was performed using Infinite M1000 instrument (Tecan, USA). The obtained data was linearized and used to calculate unknown released drug concentration (Figure B.1).

3.2.6.2 Drug Release Analysis

4 mL of FBS coated Dox encapsulated PLGA NSs at pH 7.4, 4 mL of human plasma coated Dox encapsulated PLGA NSs at pH 7.4 and 4 mL of non-coated-Dox encapsulated PLGA NSs at pH 7.4 were collected after PC formation experiment. Their Dox absorbance values were measured by the microplate reader as triplicates. 3 mL samples were poured inside the dialysis membrane (MWCO 6000-8000) that were placed into the beaker containing 0.01 M sodium phosphate buffer at pH 7.4. The temperature of the buffer was set up at 37 °C and it was stirred at 200 rpm [71]. 500 μL sample was taken from the dialysis membrane at certain intervals. Dox absorbance

was measured from taken samples as triplicates, followed by pouring back the samples inside the membrane. The concentration of remaining Dox in PLGA NSs was calculated using the Dox calibration curve at pH 7.4.

4. RESULTS and DISCUSSION

4.1 Characterization Results of PLGA Nanoparticles

Two different PLGA NSs and three different PLGA NCs were characterized according to the their solid content analysis, size, and PDI measurement, zeta potential analysis, morphological characterization, centrifugation and solid content of centrifuged samples.

4.1.1 Solid Content Analysis

Solid content analysis was carried out in order to understand how much material was lost during synthesis and how successful the synthesis was. The amount of initial solid, freeze-dried solid and solid content (wt%) were seen in Table 4.1. The amount of PLGA 2 NSs synthesized using ethyl acetate was higher than in PLGA 1 NSs synthesized using chloroform. As a result, less material was lost, leading to more efficient synthesis. When the solid content of PLGA 4 and PLGA 5 was compared, the increase in the amount of material used resulted in an increase in material loss.

Table 4.1: Solid Content of Synthesized PLGA NPs

Sample	Amount of Initial Solid (mg)	Amount of Freeze-dried Solid (mg)	Solid Content (wt%)
PLGA 1	250	231.7	2.32
PLGA 2	250	244.3	2.44
PLGA 3	460	373.6	3.74
PLGA 4	675	558.8	5.58
PLGA 5	450	445.7	4.45

4.1.2 Size and Polydispersity Index Measurement

The size and PDI results of two different NSs and three different NCs synthesized under different conditions are given below in Table 4.2. PLGA 1 and PLGA 2 NSs were separated according to the used organic solvent during the synthesis. The difference in the polarities of the organic solvents used also caused a difference in the sizes of the synthesized NPs [72]. It was observed that the size of PLGA 2 was smaller than the size of PLGA 1 whereas PLGA 1 NSs were more uniform than PLGA 2 NSs as can be seen from the polydispersity indices representing the size distribution of NSs in Table 4.2

The impact of different surfactants with different charges on the size of NCs was investigated using an anionic SDS surfactant and a non-ionic PVA surfactant. PLGA 3 NCs were synthesized using SDS whereas PLGA 4 NCs were fabricated using PVA. The size of the NCs was noticeably smaller when an anionic SDS surfactant was used. The same result was obtained when the PDI values were compared. The size distribution of the fabricated NCs using anionic SDS was closer to each other.

Last, PLGA 4 and PLGA 5 NCs were synthesized using different amounts by keeping the ratio between polymer, surfactant, and oil the same. It was noted that the size and PDI did not significantly alter as a result of the quantity variation. Nevertheless, the size distribution of PLGA 5 increased when the amount of PVA was reduced.

Table 4.2: Size and PDI of Synthesized PLGA NPs

Sample	Size (nm)	PDI
PLGA 1	258.4 ± 1.76	0.085 ± 0.01
PLGA 2	158.9 ± 0.85	0.165 ± 0.01
PLGA 3	197.2 ± 0.75	0.098 ± 0.006
PLGA 4	312.5 ± 2.34	0.172 ± 0.04
PLGA 5	294.8 ± 4.02	0.208 ± 0.032

4.1.3 Zeta Potential Analysis

The zeta potentials of all PLGA NSs and NCs were measured, as the zeta potential is a significant feature indicating the surface charge (Table 4.3). The zeta potential results are important since the situation of NSs in the blood circulation and their interaction with the cells will change depending on whether the surface is more negative or positive.

Since non-ionic PVA was used as the surfactant in the synthesis of PLGA 1, PLGA 2, PLGA 4 and PLGA 5, their surfaces were covered with PVA. This was the reason why the zeta potentials of these four samples are close to each other. Except for PVA, SDS was used as the surfactant. Since SDS is an anionic surfactant, the surface of PLGA 3 was significantly more negatively charged than the surface of other samples. A more negative surface will alter the type and amount of proteins adhered to the surface in the interaction of these NCs with blood.

Table 4.3: Zeta Potential of PLGA NPs

Sample	Zeta Potential (mV)
PLGA 1	-9.51 ± 0.74
PLGA 2	-11 ± 0.62
PLGA 3	-52.1 ± 1.75
PLGA 4	-7.89 ± 0.54
PLGA 5	-5.22 ± 0.41

4.1.4 Morphological Characterization

Morphological characterization of the samples was performed using both TEM and SEM. The TEM images of PLGA NSs and NCs at 1 μm scale are seen in Figure 4.1. PLGA 1 and PLGA 2 NSs had a perfectly spherical shape morphology. The contrast between the core and shell was observed in the TEM image of PLGA 3, PLGA 4 and PLGA 5 NCs.

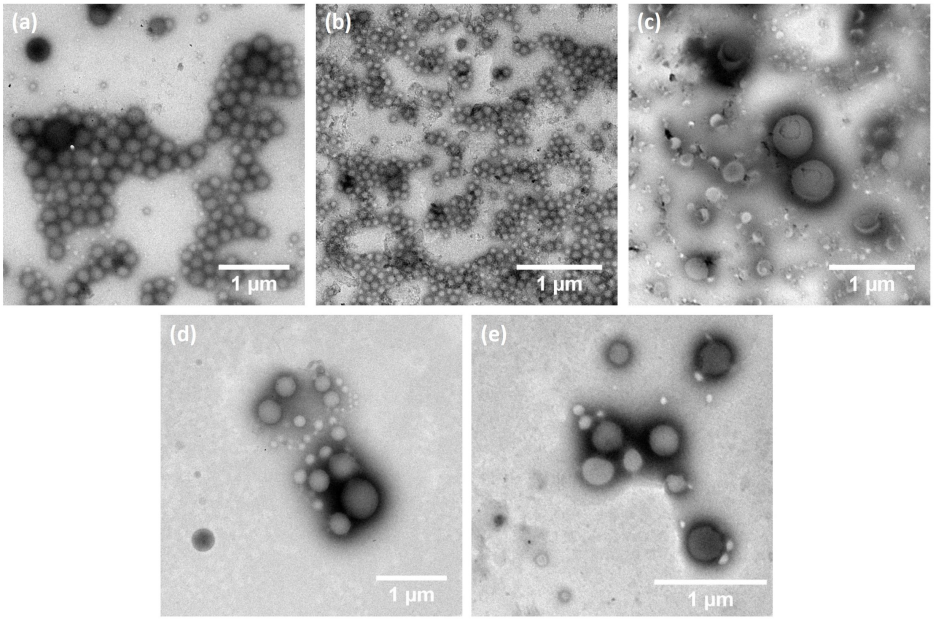

Figure 4.1: TEM Images of PLGA NPs at 1 μm scale, (a) PLGA 1, (b) PLGA 2, (c) PLGA 3, (d) PLGA 4, (e) PLGA 5

The morphologies of the samples were also imaged by SEM. The spherical structures of NSs and hollow morphology of NCs are observed in Figure 4.2. The hollow morphology of the core structure of the PLGA NCs was clearly imaged by the honeycomb image.

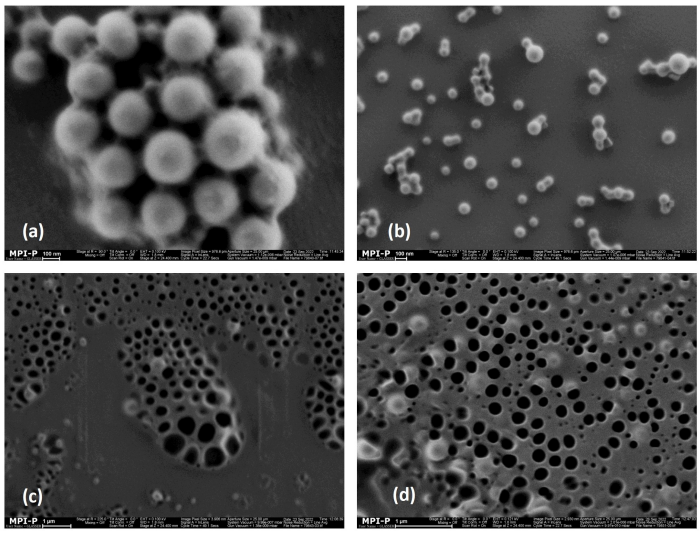

Figure 4.2: SEM Images of PLGA NPs, (a) PLGA 1 at 100 nm scale, (b) PLGA 2 at 100 nm scale, (c) PLGA 4 at 1 μm scale, (d) PLGA 5 at 1 μm scale

4.1.5 Centrifugation

Before starting the PC experiments, the samples were centrifuged three times, and then, their sizes, PDI and zeta potentials were measured to examine their stability and redispersion ability (Table 4.4). PLGA 3 NCs were barely redispersed after the first two centrifuges. However, they could not be redispersed after the third centrifugation and the non-redispersed pellet remained at the bottom of the Eppendorf (Figure 4.3). This aggregate showed that these NCs were not a suitable candidate for the PC experiment as the PC experiment comprises lots of centrifugation steps.

The obtained result when comparing the size, PDI, and zeta potential of synthesized samples and centrifuged samples showed that PLGA 1, PLGA 2, PLGA 4, and PLGA 5 were still stable and their structure did not break down after centrifugation three times at 4 °C, 20.000 g for 1 hour.

Table 4.4: Size, PDI and Zeta Potential of Centrifuged PLGA NPs

Sample	Size (nm)	PDI	Zeta Potential (mV)
PLGA 1	254.8 ± 3.63	0.078 ± 0.013	-13.3 ± 0.15
PLGA 2	160.5 ± 2.8	0.149 ± 0.018	-14.8 ± 0.57
PLGA 4	374.2 ± 9.73	0.161 ± 0.065	-7.75 ± 0.25
PLGA 5	331.9 ± 4.29	0.236 ± 0.045	-10 ± 0.73

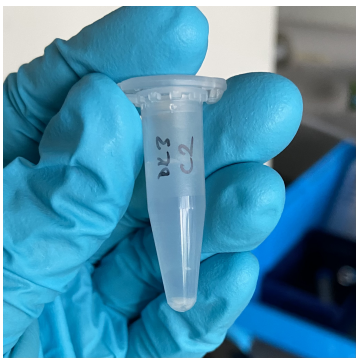

Figure 4.3: Non-redispersed pellet of PLGA 3

4.1.6 Solid Content Analysis of Centrifuged Nanoparticles

The solid contents of PLGA 1, PLGA 2, PLGA 4 and PLGA 5 were investigated after the third centrifugation to determine how many samples were lost during centrifugation (Table 4.5). While PLGA 2 and PLGA 5 had the highest sample loss, PLGA 1 had the lowest loss.

Table 4.5: Solid Content of Centrifuged PLGA NPs

Sample	Amount of Centrifuged Sample	Solid Content (wt%)	Lost (%)
PLGA 1	9.19	0.92	60.33
PLGA 2	7.60	0.76	68.86
PLGA 4	19.81	1.98	64.55
PLGA 5	13.51	1.35	69.67

4.2 Characterization Results of PCL Nanoparticles

PCL NSs were synthesized using only chloroform as an organic solvent since PCL is insoluble in ethyl acetate at room temperature. SDS was not used in PCL NC synthesis as PLGA NCs synthesized using SDS could not be redispersed after centrifugation. Since the size of PLGA 5 was slightly smaller than PLGA 4, the synthesis of PCL NCs was performed based on the amounts of PLGA 5. Subsequently, PCL NSs and NCs were characterized according to the same titles in PLGA NSs and NCs.

4.2.1 Solid Content Analysis

The amount of initial solid, freeze-dried solid and solid content (wt%) were given below in Table 4.6. When PLGA 1 and PCL 1 synthesized under the same conditions were compared, it was revealed that less material loss occurred in PCL synthesis. However, compared to PCL 2, the material loss in PLGA 5 was substantially lower.

Table 4.6: Solid Content of Synthesized PCL NPs

Sample	Amount of Initial Solid (mg)	Amount of Freeze-dried Solid (mg)	Solid Content (wt%)
PCL 1	250	243.2	2.43
PCL 2	450	412.7	4.12

4.2.2 Size and Polydispersity Index Measurement

Since PCL 1 was in NS structure, its size was smaller than PCL 2 which had NC morphology (Table 4.7). Although the difference is not much, the size of PCL 1 was slightly larger than the size of PLGA 1 when they were compared. Furthermore, their PDI was close to each other. The same difference in size was also observed between PCL 2 and PLGA 5. The size of PLGA 5 was 294.8 nm, whereas the size of PCL 2 was 366 nm. However, size distribution of PCL 2 was narrower. Its PDI was 0.157 while the PDI of PLGA 5 was 0.208.

Table 4.7: Size and PDI of Synthesized PCL NPs

Sample	Size (nm)	PDI
PCL 1	274.7 ± 2.32	0.091 ± 0.02
PCL 2	366 ± 1.56	0.157 ± 0.042

4.2.3 Zeta Potential Analysis

PVA was used as surfactant both in the synthesis of PCL 1 and in the synthesis of PCL 2. Therefore, the zeta potential of the two was similar to each other (Table 4.3). Although the same amount of PVA was used in PCL 1 and PLGA 1, the surface charge of PLGA 1 was more negative. The same situation was observed between PLGA 5 and PCL 2. The surface charge of PCL 2 was closer to zero. This difference impacts the variety and amount of protein in the PC structure. As a consequence of this impact, how long these two different kinds of NSs and NCs stay in the bloodstream and interaction between them and cells alter. Therefore, this difference in surface charges was an important parameter.

Table 4.8: Zeta Potential of PCL NPs

Sample	Zeta Potential (mV)
PCL 1	-1.50 ± 0.11
PCL 2	-1.86 ± 0.07

4.2.4 Morphological Characterization

PCL 1 and PCL 2 were characterized by TEM and SEM, respectively. Soft NSs and NCs were obtained after the preparation of samples for TEM and SEM imaging because of the physicochemical properties of PCL. The hollow capsule morphology for nanocapsules and polymeric matrix for nanospheres were seen as in Figures 4.4 and 4.5.

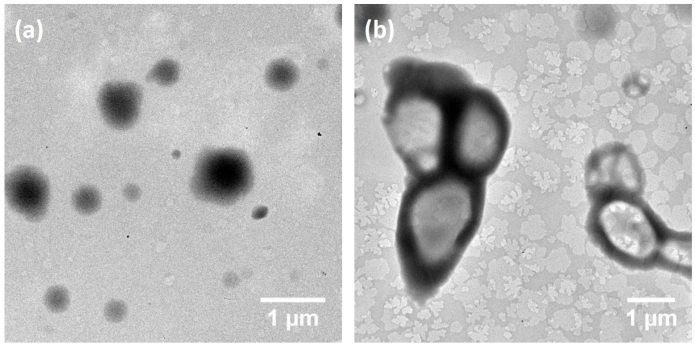

Figure 4.4: TEM Images of PCL NPs at 1 μm scale, (a) PCL 1, (b) PCL 2

PCL NSs were seen in SEM images (Figure 4.5 (a)). Furthermore, the hollow morphology of PCL NCs was observed in Figure 4.5 (b).

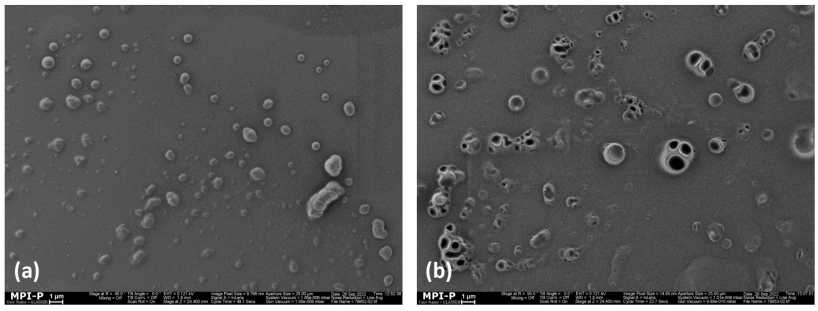

Figure 4.5: SEM Images of PCL NPs at 1 μm scale, (a) PCL 1, (b) PCL 2

4.2.5 Centrifugation

PCL samples were centrifuged three times at 4 °C, 20.000 g for 1 hour as in PLGA samples to examine their stability after centrifugation. However, it was observed that when PCL samples were centrifuged once at 4 °C, 20.000 g for 1 hour, aggregates formed (Figure 4.6).

Therefore, the centrifugation conditions were changed to 4 °C, 15.000 g for 30 minutes. After centrifugation of PCL 1 at 4 °C, 15.000 g for 30 minutes, there were not any aggregates. Thus, these centrifugation conditions were kept fixed, and they were centrifuged three times. Afterward, the size, PDI and zeta potential of centrifuged PCL 1 were determined (Table 4.9).



Figure 4.6: Aggregates of PCL 1 (a) and PCL 2 (b) after Centrifugation at 4 °C, 20.000 g for 1 hour

Table 4.9: Size, PDI and Zeta Potential of Centrifuged PCL 1

Sample	Size (nm)	PDI	Zeta Potential (mV)
PCL 1	264.8 ± 3.35	0.062 ± 0.01	-3.36 ± 0.28

On the other hand, this condition was not suitable for PCL 2 because there were still aggregates of PCL 2 after centrifugation. After this result, PCL 2 was centrifuged at 4 °C, 10.000 g for 30 minutes. It was observed that there were again PCL 2 aggregates. Lastly, they were centrifuged at 4 °C, 5000 g for 30 minutes, and aggregate formation was still seen. The size, PDI and zeta potentials of PCL 2 at three different centrifugation conditions were given below in Table 4.10.

Table 4.10: Size, PDI and Zeta Potential of Centrifuged PCL 2

Sample	Size (nm)	PDI	Zeta Potential (mV)
PCL 2 (at 15.000 g)	704.6 ± 9.21	0.054 ± 0.041	-4.09 ± 0.13
PCL 2 (at 10.000 g)	748.3 ± 141.6	0.757 ± 0.129	-
PCL 2 (at 5000 g)	744.8 ± 5.65	0.406 ± 0.02	-

4.2.6 Solid Content Analysis of Centrifuged Samples

Solid content of the three times centrifuged PCL 1 was determined to understand how much PCL 1 was lost during centrifugation (Table 4.11). On the other hand, it was not performed for centrifuged PCL 2 because PCL 2 was not stable in all three different centrifugation conditions.

Table 4.11: Solid Content of Centrifuged PCL NPs

Sample	Amount of Centrifuged Sample	Solid Content (wt%)	Lost (%)
PCL 1	5.21	0.52	78.57

4.3 Analysis of Protein Corona on PLGA Nanospheres

Protein corona (PC) coating was performed using FBS or human plasma to determine which proteins could interact with NSs.

Human plasma was taken from ten healthy donors at the Department of Transfusion Medicine Mainz (Germany). Taken plasma was pooled and stored at -20 °C until used.

PC experiments were continued with PLGA 1 (Table 3.1) and PCL 1 (Table 3.2) NSs, which were synthesized using chloroform as the organic solvent, to keep all conditions similar. A constant surface area was chosen to compare the interaction between different NSs and proteins. For this purpose, 0.05 m^2 surface area was fixed,

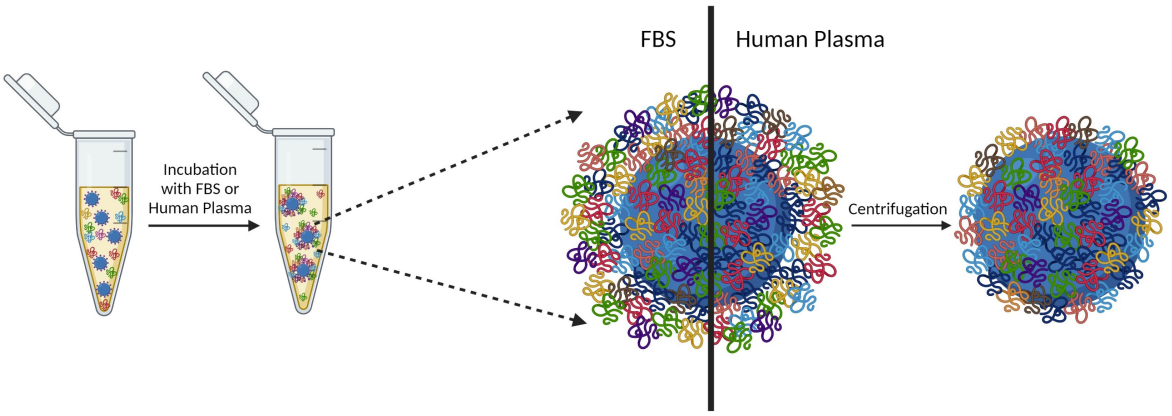

Figure 4.7: Formation of PC Structure on NS Surface

and the required volume for 0.05 m^2 surface area of NSs was calculated. As a result of the calculations, 142.22 μL of PLGA 1 corresponded to NSs with a surface area of 0.05 m^2. PC coated PLGA 1 NSs were characterized regarding size, PDI and zeta potential.

4.3.1 Size and Polydispersity Index Measurement

PLGA 1 was incubated with FBS or human plasma for the formation of the PC layer around the surface. As the control group, PLGA 1 was incubated with only PBS. The SPC was formed during incubation at 37 °C, 300 rpm to mimic the bloodstream conditions. After incubation, they were centrifuged to remove unbound or weakly bound proteins. They were redispersed in PBS after each centrifugation step. When the fourth centrifugation was completed, HPC coated PLGA 1 was obtained and characterized with respect to size and PDI (Table 4.12). It was determined that the size of the NSs interacting with the proteins was bigger than the size of the NSs in the control group. Besides, since there were proteins around the surface of NSs, the PDI of PC coated PLGA 1 NSs was higher than the control group. This situation was expected because proteins of different sizes would affect the size distribution.

Table 4.12: Size and PDI of PC Coated PLGA 1 NSs

Characterization	Human Plasma Coated PLGA 1 NSs	FBS Coated PLGA 1 NSs	Control Group of PLGA 1 NSs
Size (nm)	273.2 ± 3	279.9 ± 2.56	265 ± 3.83
PDI	0.074 ± 0.045	0.086 ± 0.013	0.046 ± 0.03

4.3.2 Zeta Potential Analysis

The zeta potential results of PC coated PLGA 1 NSs and PLGA 1 NSs in the control group were identified after the fourth centrifugation (Table 4.13). Their zeta potential was similar to each other; however, the zeta potential of the control group was slightly more negatively charged. The reason why the zeta potentials were so close to each other was that there was more than one protein in the HPC structure. Since the charge of each of the proteins in this structure was different from each other, the charge of the HPC structure they formed together was not much different from the surface charge of the control group.

Table 4.13: Zeta Potential of PC Coated PLGA 1 NSs

Characterization	Human Plasma Coated PLGA 1 NSs	FBS Coated PLGA 1 NSs	Control Group of PLGA 1 NSs
Zeta Potential (mV)	-13.6 ± 0.55	-13.9 ± 0.36	-14.7 ± 0.05

4.3.3 Protein Assay

The supernatant of each centrifugation was collected to calculate the concentration of removed proteins. After the fourth centrifugation, the NSs were incubated with a desorption buffer containing SDS and then centrifuged to break the bonds between the NSs and the proteins in the HPC. In this way, the proteins forming the HPC structure were obtained. The absorbance values of the supernatants at 660 nm were obtained and the concentrations of the proteins were calculated by fitting their absorbance values to the BSA calibration curve seen in Figure A.1. Table 4.14 showed the

absorbance and concentration results of proteins found in FBS supernatants whereas the results of proteins found in human plasma supernatants were given in Table 4.15. It was found that the concentration of proteins found in the HPC of human plasma was much higher.

Table 4.14: Absorbance and Concentration Values of Proteins in FBS Supernatants of PLGA NSs

Sample	Absorbance (660 nm)	Concentration (μg/mL)
FBS	2.13 ± 0.91	5374.25 ± 2286.95
FBS Soft PC	1.72 ± 0.62	4319.91 ± 1549.51
FBS Wash 1	0.93 ± 0.35	2344.33 ± 891.51
FBS Wash 2	0.03 ± 0.01	104.92 ± 27.70
FBS Wash 3	0.01 ± 0.01	50.66 ± 30.90
FBS Hard PC	0.013 ± 0.01	59.16 ± 15.66

Table 4.15: Absorbance and Concentration Values of Proteins in Human Plasma Supernatants of PLGA NSs

Sample	Absorbance (660 nm)	Concentration (μg/mL)
Human Plasma	1.32 ± 0.55	3323.75 ± 1372.17
Human Plasma Soft PC	0.90 ± 0.27	2284.75 ± 681.56
Human Plasma Wash 1	0.88 ± 0.009	2231.16 ± 22.30
Human Plasma Wash 2	0.06 ± 0.01	180.33 ± 30.52
Human Plasma Wash 3	0.02 ± 0.003	63.42 ± 9.02
Human Plasma Hard PC	0.03 ± 0.004	112.66 ± 9.98

4.3.4 SDS-PAGE

It was determined how many μg of samples would be loaded on the gel for SDS-PAGE according to the obtained protein concentrations. In samples with FBS, 2.6 μg FBS, 2 μg Soft PC, 1 μg Wash 1, 1 μg Wash 2, 1 μg Wash 3 and 1 μg Hard PC were loaded onto the gel. For samples with human plasma, it was determined as 1.6 μg human plasma, 2 μg Soft PC, 2 μg Wash 1, 2 μg Wash 2, 2 μg Wash 3, and 2 μg Hard PC. Images of silver-stained gels were given in Figure 4.8.

It was clear that most of the proteins were removed after the first centrifugation, comparing FBS and its SPC or human plasma and its SPC. It was obviously detected that there was a decrease in the amount of protein after each centrifugation because the bands diminished which was also proved by protein quantification.

In addition, it was determined that the proteins in the HPC layers had a broad molecular weight distribution since their gel images contained bands in the range of 28 to 198 kDa.

When these two gel images were compared, it was seen that both HPCs have a clear and thin band at 62 kDa which referred to the serum albumin band. There were more bands at the 28 kDa molecular weight range in the HPC of human plasma. This means that in the HPC of human plasma there was more protein with a molecular weight close to 28 kDa. This range was also important since apolipoprotein E and apolipoprotein A-I, which are in the de-opsonin group, have molecular weights in these ranges.

Moreover, there was a distinct band above 198 kDa in both SDS-PAGE gels, which was expected to refer to apolipoprotein B-100, which has approximately 515 kDa. The band below 198 kDa in both gels could be the band formed by the complement C3. Complement C3 is an important protein among the proteins that make up the complement system. Fibrinogen alpha chain, beta chain and gamma chain, which have weights of 95, 56, and 51 kDa, respectively, are the most abundant proteins in the coagulation group. Therefore, these proteins were expected to be present in both HPC structures. Some of the bands between 98 to 49 kDa were predicted to indicate these three proteins.

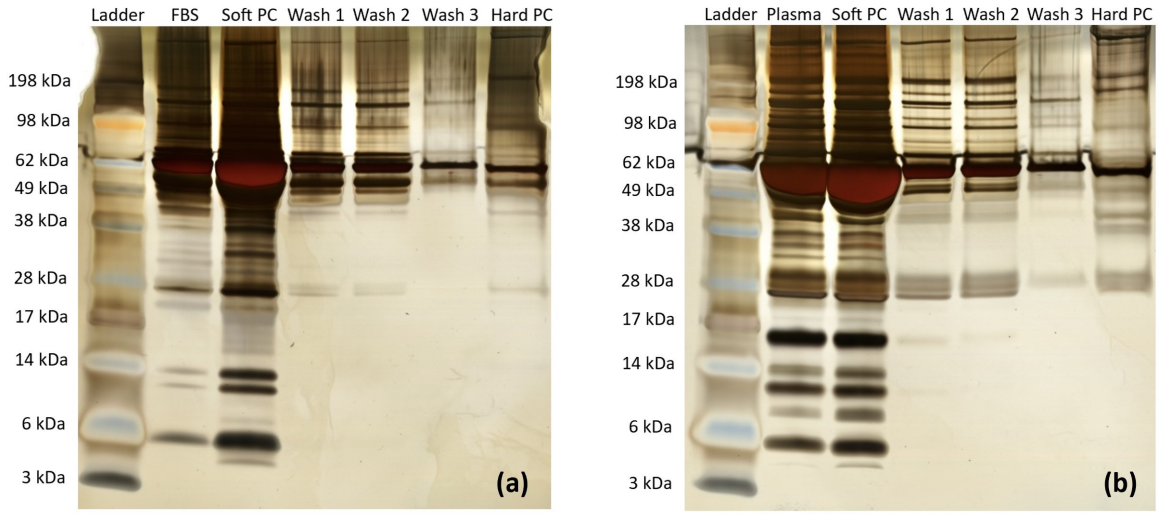

Figure 4.8: Silver Stained SDS-PAGE Gels of PC Structure of PLGA 1 NSs, (a) Proteins in FBS PC, (b) Proteins in Human Plasma PC

4.3.5 Liquid Chromatography-Mass Spectrometry

Since SDS-PAGE performs the qualitative analysis of proteins in the HPC, LC-MS is a significant method to identify individual proteins. First of all, SDS, which was used to break down the interaction between NSs and proteins in the HPC, was removed in the process of preparing samples for liquid chromatography-mass spectrometry. Afterward, proteins were precipitated and digested using trypsin. During the measurement, Glu-Fibrinopeptide and Leu-Enkephalin were used as the reference peptides. Protein identification from both FBS HPC and human plasma HPC was conducted in triplicate.

After the amount (fmol) of each of these proteins in the HPC was calculated, it was established what percentage of this structure they constituted. Subsequently, all proteins were grouped (lipoproteins, complement system or coagulation, etc.) according to their type (Figure 4.9 (a)). Proteins predicted by SDS-PAGE were confirmed by the LC-MS technique. The 20 most abundant proteins in both structures were listed to compare proteins in both human plasma and FBS HPC (Figure 4.9 (b)).

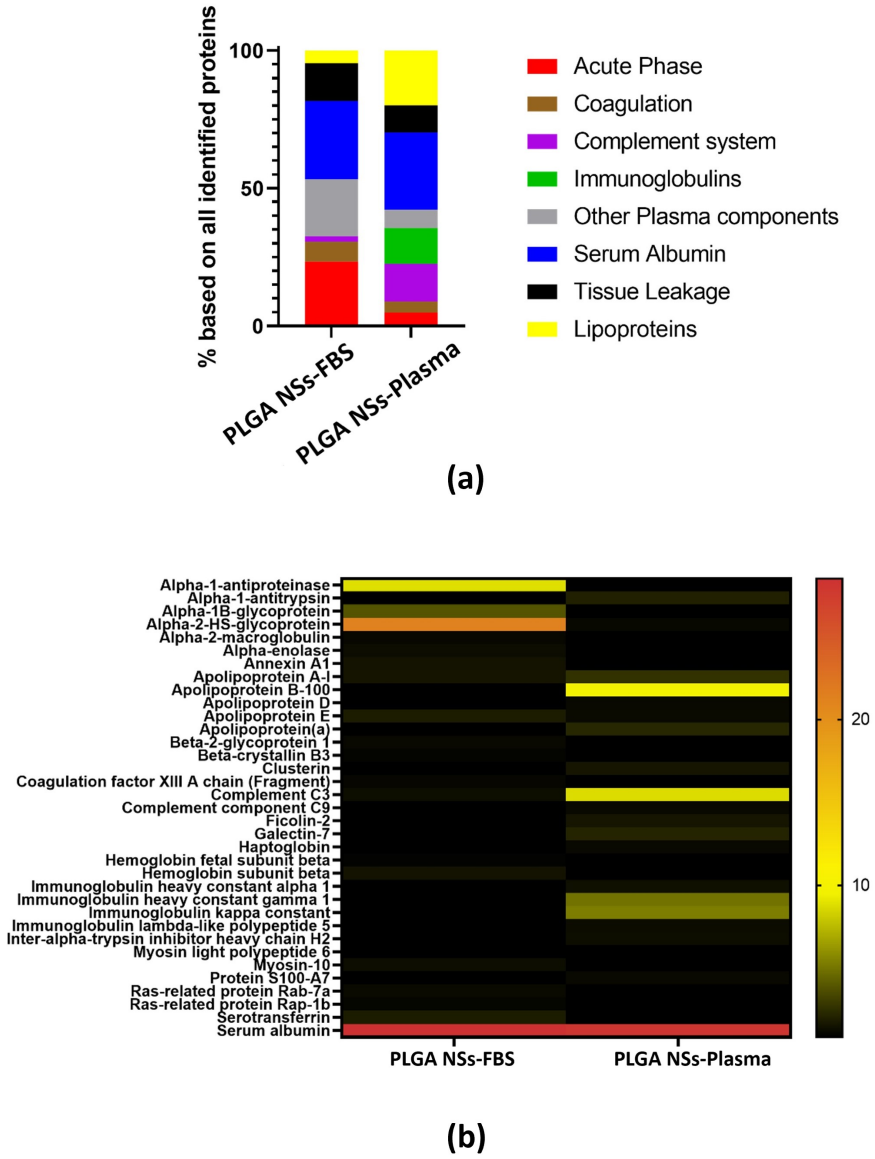

Figure 4.9: Liquid Chromatography-Mass Spectrometry Results, (a) Grouping of Proteins in HPC of PLGA NSs, (b) The Most Abundant Proteins in both Human Plasma and FBS HPC

It was observed as a result of protein grouping that serum albumin constituted most of both structures. Lipoproteins, which are important dysopsonins, were the second most abundant group in human plasma samples. However, the second most common group in FBS samples was the acute phase group which is a member of opsonins. Another important difference was the absence of immunoglobulins in the FBS samples. This difference is one of the key distinctions between FBS and human plasma.

There were five proteins that were common in both FBS and human plasma HPC structure. These proteins were serum albumin, apolipoprotein A-I and apolipoprotein E, which formed dysopsonins, and complement C3 and alpha-2-HS-glycoprotein, which constituted opsonins. When the amounts of these proteins in the structure are compared, 28% of both structures are composed of serum albumin. Complement C3 comprised 8% of the human plasma HPC, while the proportion in FBS HPC was around 1.5%. Apolipoprotein E was found at approximately 1.5% of the human plasma structure and 2% of the FBS structure, respectively. The ratio of apolipoprotein A-I was similar in both structures; approximately 3% of the human plasma structure and 2% of the FBS structure. Nevertheless, alpha-2-HS-glycoprotein, a member of the acute phase, constituted 1.2% of the human plasma structure and 22% of the FBS structure.

In human plasma samples, it was determined that the percentage of dysopsonins, which extends the blood circulation time of NSs by providing the NSs stealth feature, was 47.95% wherease opsonins, which cause the NSs to be cleared from the body by triggering the immune system cells, had 35.5%. This difference in rate is important in terms of increasing the circulation times of PLGA NSs in the blood. Nonetheless, this ratio was very close to each other in FBS samples. Dysopsonins formed by lipoproteins and serum albumin were found in 33.1%, while the rate of opsonins formed by coagulation, acute phase and complement system was 32.5%. The difference between these two ratios in human plasma and FBS indicated that the HPC of human plasma could not be adequately mimicked by FBS.

4.4 Analysis of Protein Corona on PCL Nanospheres

As a consequence of calculations, 107.86 μL of PCL 1 corresponded to NSs with a 0.05 m^2 surface area. PC coated PCL 1 NSs were characterized in regard to the size, polydispersity and zeta potential. In addition, PC structure was analyzed regarding protein assay, SDS-PAGE and LC-MS.

4.4.1 Size and Polydispersity Index Measurement

After PCL 1 NSs were incubated with either FBS or human plasma, they were centrifuged four times to eliminate unbound proteins and acquire the HPC coated PCL 1 NSs. The size and PDI of HPC coated PCL 1 NSs were determined by DLS (Table 4.16). The size of the NSs in the control group, in which all the steps were applied under the same conditions without FBS or human plasma, was 290.6 nm, while the size of the HPC coated NSs was bigger. The size of FBS-coated PCL 1 was 293.4 nm, whereas the size of human plasma-coated PCL 1 was 295.7 nm.

The change in the PDI of the PC coated NSs was also evident. The PDI of the NSs in the control group was 0.023. However, the PDI of the FBS coated NSs was 0.095, due to the different types and different amounts of proteins present on the PC coated NSs' surface. The PDI of the NSs coated with human plasma was 0.049.

When comparing both PLGA 1 and PCL 1 NSs coated with HPC, it was observed that the average size of those NSs coated with human plasma was bigger than the average size of NSs coated with FBS.

Table 4.16: Size and PDI of PC Coated PCL 1 NSs

Characterization	Human Plasma Coated PCL 1 NSs	FBS Coated PCL 1 NSs	Control Group of PCL 1 NSs
Size (nm)	295.7 ± 5.77	293.4 ± 4.29	290.6 ± 2.4
PDI	0.049 ± 0.038	0.095 ± 0.043	0.023 ± 0.004

4.4.2 Zeta Potential Analysis

The zeta potentials of the HPC coated NSs and the NCs in the control group were identified by ELS (Table 4.17). The surface charge of all three was similar. The reason for this was that, as mentioned in Section 4.2.1.2, there were many proteins in the HPC structure and the charges of the proteins were different from each other.

Table 4.17: Zeta Potential of PC Coated PCL 1 NSs

Characterization	Human Plasma Coated PCL 1 NSs	FBS Coated PCL 1 NSs	Control Group of PCL 1 NSs
Zeta Potential (mV)	-4.5 ± 0.243	-4.61 ± 0.131	-4.63 ± 0.37

4.4.3 Protein Assay

Supernatants obtained after each centrifugation were collected and stored for the determination of protein concentrations. In order to break the bond between the proteins in the HPC layer and the NSs, the NSs were incubated with a desorption buffer containing SDS at 95 °C and then centrifuged for the last time. The protein absorbances of all supernatants were measured at 660 nm. Their concentrations were then calculated by fitting the previously prepared BSA curve (Figure A.1). The absorbance and concentration results of FBS supernatants were given in Table 4.18, while the absorbance and concentration results of human plasma supernatants were given below in Table 4.19.

The FBS concentration was higher than that of human plasma; however, the protein concentration in the FBS HPC layer was lower. Since PC experiments were performed by keeping all conditions the same, this meant that there was a higher concentration of protein in the HPC covered with human plasma.

Table 4.18: Absorbance and Concentration Values of Proteins in FBS Supernatants of PCL 1 NSs

Sample	Absorbance (660 nm)	Concentration (μg/mL)
FBS	1.79 ± 0.41	4500.49 ± 1028.44
FBS Soft PC	1.31 ± 0.48	3303.83 ± 1209.75
FBS Wash 1	0.45 ± 0.10	1139.33 ± 257.96
FBS Wash 2	0.04 ± 0.01	124.41 ± 20.69
FBS Wash 3	0.03 ± 0.01	94.16 ± 16.83
FBS Hard PC	0.01 ± 0.01	53.41 ± 20.61

Table 4.19: Absorbance and Concentration Values of Proteins in Human Plasma Supernatants of PCL 1 NSs

Sample	Absorbance (660 nm)	Concentration (μg/mL)
Human Plasma	0.82 ± 0.82	2079.66 ± 226.40
Human Plasma Soft PC	0.65 ± 0.03	1671.16 ± 77.70
Human Plasma Wash 1	0.75 ± 0.07	1905.83 ± 167
Human Plasma Wash 2	0.06 ± 0.01	174.92 ± 35.03
Human Plasma Wash 3	0.03 ± 0.01	104.33 ± 21.42
Human Plasma Hard PC	0.02 ± 0.01	86.91 ± 30.90

4.4.4 SDS-PAGE

The amount of protein to be used for SDS-PAGE was determined according to the obtained concentration values. For analysis of FBS samples, 1 μg FBS, 1 μg Soft PC, 1 μg Wash 1, 1 1 μg Wash 2, 2 μg Wash 3 and 1 μg Hard PC were loaded onto the gel. For the analysis of human plasma, 1 μg human plasma, 0.5 μg Soft PC, 2 μg Wash 1, 2 μg Wash 2, 2 μg Wash 3 and 3.4 μg Hard PC samples were prepared. After the gels were run at a constant 100 Volt for 1 hour, they were stained by silver staining and imaged (Figure 4.10).

When imaged two gels were compared, it was observed that bands of proteins, which had higher molecular weights, were more in the HPC formed using human plasma. One of the bands above 198 kDa obtained in both gels was expected to be apolipoprotein B100. Other bands obtained in this range in human plasma were estimated as apolipoprotein(a) or apolipoprotein D, which are also in the lipoprotein group. A band corresponding to 62 kDa was observed in both HPC structures. This band was most likely the band formed by serum albumin proteins. In the HPC of human plasma, the bands referred to the low molecular weight range were observed. Bands between 28 and 49 kDa could represent some proteins from the lipoprotein group as well as some proteins from the immunoglobulins group. Among the lipoproteins, apolipoprotein A-I, apolipoprotein A-II, apolipoprotein A-IV, apolipoprotein D, apolipoprotein E and clusterin are in these molecular weight ranges. Complement C3,

complement C4, and complement C7 proteins are found in the range of 98 to 198 kDa, which are important complement system members in the innate immune system. Thus, it was significant to learn individually which proteins were in these ranges.

In addition, it was seen that many proteins were removed after the first centrifugation when FBS and its Soft PC or human plasma and its Soft PC were compared. Each centrifugation step ensured of removal of slightly bound proteins. Thus, proteins that bind tightly to NPs were obtained and examined.

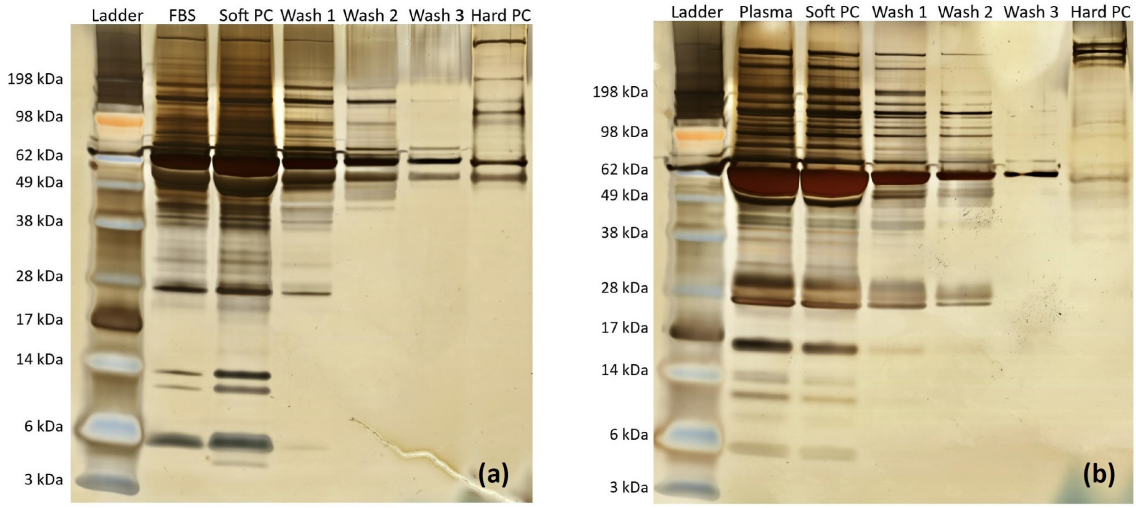

Figure 4.10: Silver Stained SDS-PAGE Gels of PC Structure of PCL 1 NSs, (a) Proteins in FBS PC, (b) Proteins in Human Plasma PC

4.4.5 Liquid Chromatography-Mass Spectrometry

The predicted proteins were individually identified and confirmed by LC-MS. Among the 20 most abundant proteins in human plasma HPC, the most important ones were apolipoprotein B-100, apolipoprotein (a), apolipoprotein A-I, apolipoprotein A-IV and clusterin from the lipoprotein group; serum albumin; complement C3, complement C4-A, complement C4-B and ficolin-2 from the complement system; immunoglobulin kappa constant, immunoglobulin heavy constant alpha 1, immunoglobulin heavy constant gamma 2 and immunoglobulin heavy constant mu from the immunoglobulins. In FBS samples, the important ones in the first 20 proteins were complement C3,

complement C4, complement component C7, and complement component C9 from the complement system; apolipoprotein E; serum albumin (Figure 4.11 (b)). Since there is no immunoglobulin in FBS, proteins from this group were not found in the HPC.

According to the result obtained when the proteins in the HPC were grouped, the most abundant group in the HPC formed by human plasma was lipoproteins (Figure 4.11 (a)). The second main group was immunoglobulins, and the third group was the complement system. The percentage of opsonins in human plasma was approximately the same as the percentage of dysopsonins. On the other hand, when the FBS HPC was grouped, the first three most abundant groups were lipoproteins, other plasma components, and the complement system, respectively. When comparing the ratio in human plasma and in FBS, there was a greater difference in the ratio between dysopsonins and opsonins in the FBS samples. However, the rate of opsonins was also quite similar to the proportion of dysopsonins in these samples as well. The fact that the ratios were almost identical to each other could make a significant difference in the cellular uptake of these NSs. This situation was also critical as it would affect the capture of the NSs by the immune system cells and their duration in the bloodstream.

Compared to the LC-MS results of PLGA NSs, PLGA NSs were more promising because of the fact that dysopsonin groups were significantly more numerous than opsonin groups. One of the most important reasons for this significant difference in the protein type and group was that the zeta potentials of PLGA and PCL NSs were different. Since the protein to be bound would vary according to the surface charge of NSs, the proteins absorbed to the surface and their ratios changed. It was anticipated that the *in vivo* fates of these two biodegradable NSs would differ from each other based on the data gained as a consequence of this research.

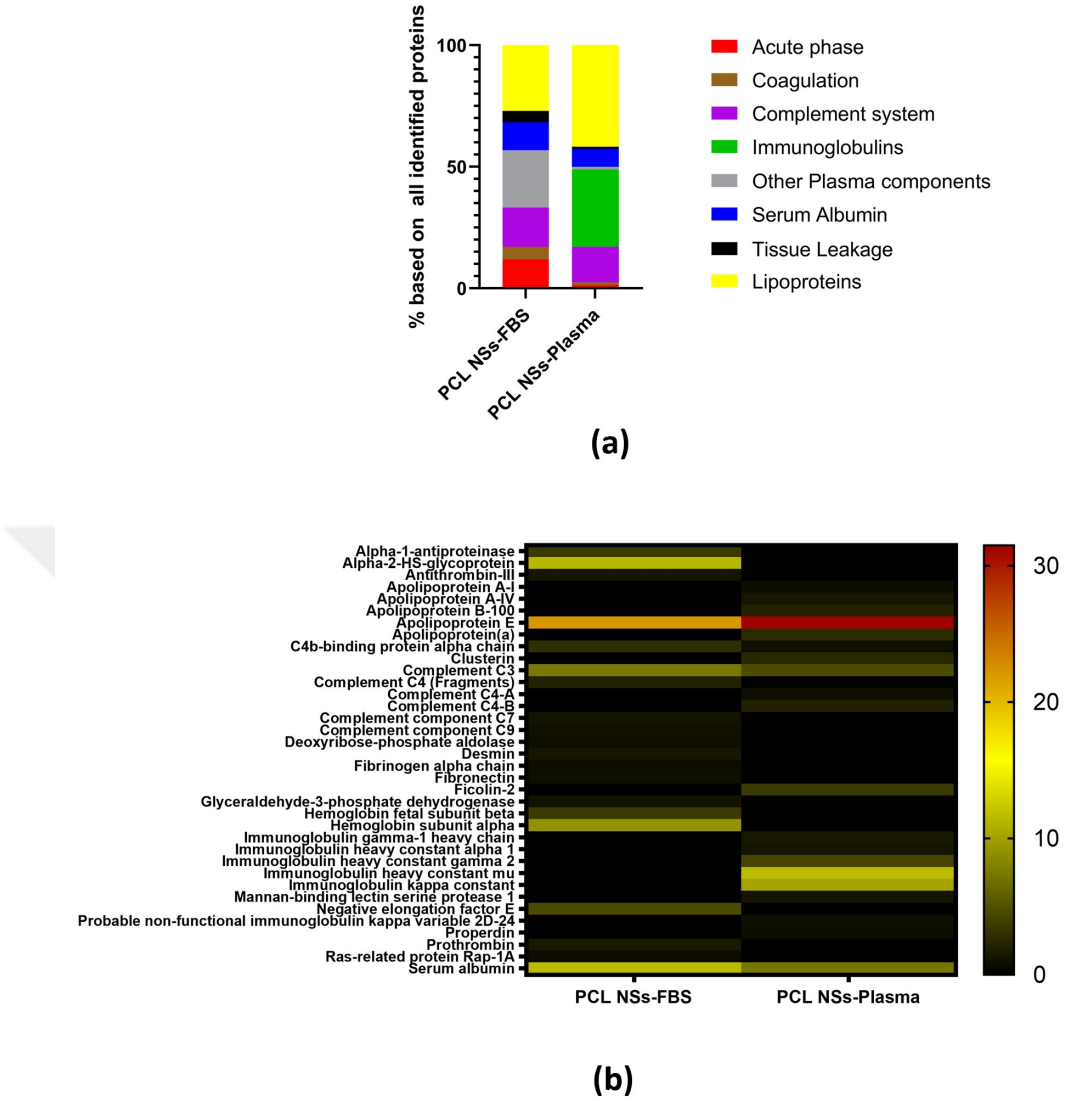

Figure 4.11: Liquid Chromatography-Mass Spectrometry Results, (a) Grouping of Proteins in HPC of PCL NSs, (b) The Most Abundant Proteins in both Human Plasma and FBS HPC

4.5 Doxorubicin Encapsulated PLGA Nanospheres

PLGA NSs were selected as application-oriented in drug release since the dysopsonin group was more in the HPC of these NSs according to LC-MS results. Dox encapsulated PLGA NSs were synthesized using 10 mg of Doxorubicin HCl (1 mg/mL). Then, they were characterized regarding size, PDI, zeta potential and encapsulation efficiency.

4.5.1 Characterization of Doxorubicin Encapsulated PLGA Nanospheres

4.5.1.1 Solid Content Analysis

The amount of initial solid and freeze-dried solid and solid content (wt%) were given in Table 4.20. This was the first of the steps that showed the synthesis was successful synthesis.

Table 4.20: Solid Content of Dox Encapsulated PLGA 1 NSs

Sample	Amount of Initial Solid (mg)	Amount of Freeze-dried Solid (mg)	Solid Content (wt%)
Dox encapsulated PLGA 1	260	2.45	2.59

4.5.1.2 Size and Polydispersity Index Measurement

After synthesis, the size and PDI of PLGA 1 NSs were determined. In addition, the stability of Dox encapsulated PLGA 1 NSs at pH 7.4 was also important, as drug release experiment would be performed at this pH value. Therefore, Dox encapsulated PLGA 1 NSs were centrifuged at 4 °C, 20.000 g for 1 hour. The pellet was redispersed in the prepared pH 7.4 Na_3PO_4 buffer. Dox encapsulated PLGA 1 NSs were stable at pH 7.4. After once centrifugation, their size and PDI did not change much. Their size obtained after synthesis was 271.9 nm whereas their size was 260.6 nm at pH 7.4 (Table 4.21). Besides, their PDI was similar to each other.

PLGA 1 NSs were 258.4 nm in size; however, the size of Dox encapsulated PLGA 1 was 271.9 nm. Encapsulation of Dox led to a slight increase in the size of the NSs.

Table 4.21: Size and PDI of Dox Encapsulated PLGA 1 NSs

Sample	Size (nm)	PDI
Dox encapsulated PLGA 1	271.9 ± 1.87	0.118 ± 0.026
Dox encapsulated PLGA 1 at pH 7.4	260.6 ± 5.08	0.078 ± 0.065

4.5.1.3 Zeta Potential Analysis

Zeta potential of synthesized Dox encapsulated PLGA 1 NSs and redispersed Dox encapsulated PLGA 1 NSs at pH 7.4 was measured by ELS. Since NSs were centrifuged at 4 °C, 20.000 g for 1 hour, some NSs were lost. Therefore, a slight difference in zeta potential occurred.

The zeta potential of PLGA 1 NSs was -9.51; however, Dox encapsulated PLGA 1 NSs had a surface charge of -2.37. These NSs had a polymeric matrix. Thus, Dox could be close to or on the surface of NPs. This situation could affect the surface charge and make a difference in the zeta potential.

Table 4.22: Zeta Potential of Dox Encapsulated-PLGA 1 NSs

Sample	Zeta Potential (mV)
Dox encapsulated PLGA 1	-2.37 ± 0.006
Dox encapsulated PLGA 1 at pH 7.4	-6.59 ± 0.6

4.5.1.4 Determination of Encapsulation Efficiency

The encapsulation efficiency was determined using the initial amount of Dox and the amount of free Dox. 10 mg of Dox was used for synthesis. Dox encapsulated PLGA 1 NSs were incubated with either human plasma, FBS or PBS. Then, non-coated NSs in the control group, or coated with human plasma or FBS were centrifuged four times at 4 °C, 20.000 g for 1 hour during the PC experiments. After each centrifugation, 4 mL of supernatants were collected and stored to determine the amount of free Dox. The absorbance of free Dox was measured at 480 nm by a microplate reader. Dox concentration of each supernatant was identified by fitting their absorbance values to the previously prepared Dox calibration curve (Figure B.1). Then, the amount of free Dox obtained after each centrifugation was calculated by multiplying the concentration by the supernatant volume. According to calculations, the encapsulation efficiency was 94.0% in human plasma coated, 95.0% in FBS coated, and 95.5% in the non-coated group (Table 4.23). This meant that NSs with a drug loading content of 0.95 mg/mL

were successfully synthesized.

Table 4.23: Encapsulation Efficiency of Dox Encapsulated PLGA 1 NSs

Sample	Encapsulation Efficiency (%)
Human Plasma Coated Dox encapsulated PLGA 1	94.0
FBS Coated Dox encapsulated PLGA 1	95.0
Dox encapsulated PLGA 1 in Control Group	95.5

4.5.2 Analysis of Protein Corona on Doxorubicin Encapsulated PLGA Nanospheres

Dox encapsulated PLGA NSs were characterized in respect of size, PDI, zeta potential, protein assay and SDS-PAGE.

4.5.2.1 Size and Polydispersity Index Measurement

Dox encapsulated PLGA 1 NSs were treated with either human plasma, FBS or PBS. After the fourth centrifugation, all three conditions were redispersed in 0.01 M pH 7.4 Na_3PO_4 buffer, followed by the measurement of the size and PDI. When the protein coated NSs were compared with the NSs in the control group, the protein coated NSs had bigger sizes and higher PDIs.

Table 4.24: Size and PDI of PC Coated Dox Encapsulated PLGA 1 NSs at pH 7.4

Characterization	Human Plasma Coated Dox Encapsulated PLGA 1	FBS Coated Dox Encapsulated PLGA 1	Control Group of Dox Encapsulated PLGA 1
Size (nm)	278.2 ± 2.35	271.7 ± 3.91	264.8 ± 3.61
PDI	0.079 ± 0.005	0.078 ± 0.009	0.057 ± 0.03

4.5.2.2 Zeta Potential Analysis

The same conditions for size and PDI measurement were applied to the zeta potential analysis. As a result of the zeta potential measurement (Table 4.25), the surface charges of all three groups were very close to each other. The reason of this situation was explained in Section 4.2.1.2.

Table 4.25: Zeta Potential of PC Coated Dox Encapsulated PLGA 1 NSs at pH 7.4

Characterization	Human Plasma Coated Dox Encapsulated PLGA 1	FBS Coated Dox Encapsulated PLGA 1	Control Group of Dox Encapsulated PLGA 1
Zeta Potential (mV)	-8.89 ± 0.18	-8.67 ± 0.22	-8.88 ± 0.37

4.5.2.3 Protein Assay

All supernatants were collected and stored to measure protein concentrations in addition to the free Dox concentration. Their absorbance values were measured at 660 nm and fitted to the BSA calibration curve (Figure A.1) to calculate corresponding concentration values (Table 4.26 and Table 4.27).

It was determined that the FBS hard protein concentration of the proteins on the Dox encapsulated PLGA NSs was 112.08 μg/mL whereas the FBS hard protein concentration of the proteins on the PLGA NSs was 59.16 μg/mL. This meant that Dox resulted in a significant increase in protein concentration of the HPC formed with FBS. The human plasma hard protein concentration was 106.92 μg/mL when it was formed around the Dox encapsulated PLGA NSs. However, the HPC concentration of human plasma on PLGA NSs was 112.66 μg/mL. The existence of Dox did not lead to a significant difference in the protein concentration of HPC formed by human plasma.

Table 4.26: Absorbance and Concentration Values of Proteins in FBS Supernatants of Dox Encapsulated PLGA 1 NSs

Sample	Absorbance (660 nm)	Concentration (μg/mL)
FBS	1.57 ± 0.21	3949.92 ± 517.98
FBS Soft PC	1.25 ± 0.07	3162 ± 172.74
FBS Wash 1	0.71 ± 0.05	1794.08 ± 128.81
FBS Wash 2	0.05 ± 0.002	150.5 ± 5.57
FBS Wash 3	0.026 ± 0.009	90.66 ± 2.32
FBS Hard PC	0.034 ± 0.003	112.08 ± 6.62

Table 4.27: Absorbance and Concentration Values of Proteins in Human Plasma Supernatants of Dox Encapsulated PLGA 1 NSs

Sample	Absorbance (660 nm)	Concentration (μg/mL)
Human Plasma	0.83 ± 0.04	2092.58 ± 95.17
Human Plasma Soft PC	0.93 ± 0.14	2364.5 ± 349.7
Human Plasma Wash 1	0.77 ± 0.05	1948.08 ± 118.26
Human Plasma Wash 2	0.054 ± 0.005	161.83 ± 12.28
Human Plasma Wash 3	0.018 ± 0.005	70.92 ± 11.72
Human Plasma Hard PC	0.032 ± 0.003	106.92 ± 7.12

4.5.2.4 SDS-PAGE

To investigate the protein distribution, 1 μg FBS, 1 μg soft PC, 1 μg wash 1, 1 μg wash 2, 2 μg wash 3 and 3 μg hard PC were loaded into the gel. In addition, 1 μg human plasma, 0.5 μg soft PC, 2 μg wash 1, 2 μg wash 2, 2 μg wash 3 and 3 μg hard PC were prepared and loaded into another gel. After running at a constant 100 V, gels were imaged (Figure 4.12).

When these two gels were compared, there were not any protein bands in the 28 kDa molecular weight range in FBS HPC. On the other hand, there was an apparent band at 62 kDa in both gel images, most likely referring to serum albumin.

Images of the FBS HPC of Dox encapsulated PLGA NSs and the FBS HPC of PLGA NSs were compared. It was found that they were quite similar to each other. Bands were observed at the same points in both images up to 49 kDa. However, when the ranges in which molecular weights of proteins lower than 49 kDa were represented were examined, it was observed that bands of lower molecular weights were not seen in the FBS HPC coated Dox encapsulated NSs. However, this distinctness could be related to the silver staining stage. As both gel images were almost identical, the bands were expected to be complement C3, serotransferrin, coagulation factor XIII A, apolipoprotein E, myosin-10, alpha-1-antiproteinase or alpha-1B-glycoprotein, which were most abundant proteins in FBS-coated PLGA NSs.

Bands in human plasma HPC coated PLGA NSs and human plasma HPC coated Dox encapsulated PLGA NSs were directly similar to each other. Exclusively, some bands in human plasma coated PLGA NSs were more apparent. The reason for this is related to the concentrations of the proteins. Since the similarity in gels in both cases indicated that the LC-MS results would be similar to each other for human plasma samples, it was expected that the bands referred to apolipoprotein B-100, apolipoprotein(a), apolipoprotein D, complement C3, complement component C9, serum albumin or clusterin. Based on this similarity, it was estimated that many of the 57 proteins obtained in the HPC of PLGA NSs were also found in the HPC of Dox encapsulated PLGA NSs.

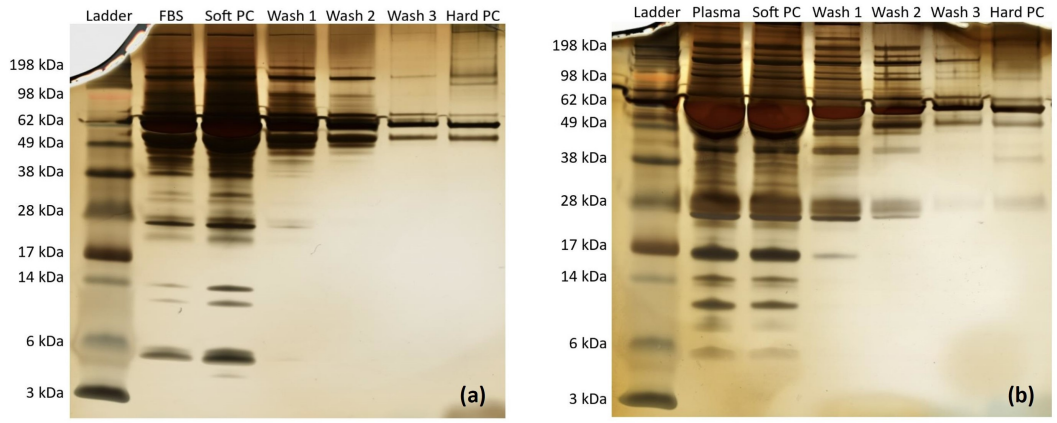

Figure 4.12: Silver Stained SDS-PAGE Gels of PC Structure of Dox Encapsulated PLGA 1 NSs, (a) Proteins in FBS PC, (b) Proteins in Human Plasma PC

4.5.3 *In vitro* Doxorubicin Release

Dox was dissolved in 0.01 M Na_3PO_4 buffer at pH 7.4 to obtain the calibration curve. Subsequently, diluted Dox samples were prepared, and their absorbance-concentration graph at 480 nm was obtained (Figure B.1).

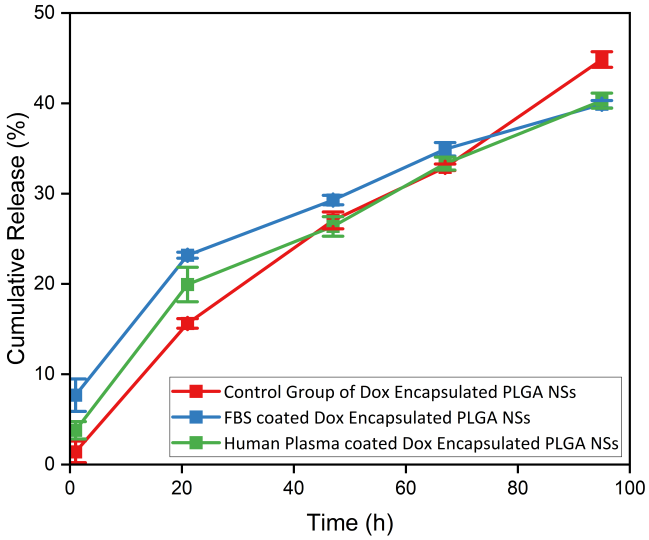

Figure 4.13: *In vitro* Doxorubicin Release from PLGA NSs at 37 °C, pH 7.4 dialysis medium

The amount of Dox in the supernatants was measured and the encapsulation efficiency was calculated in order to identify the success of the synthesis. Subsequently, Dox release from PLGA NSs was studied at 37 °C and pH 7.4 to mimic the physiological conditions. The Dox encapsulated NSs were classified into three groups as human plasma coated, FBS coated, or non-coated to identify the impact of proteins on drug release. Drug release from biodegradable PLGA NSs was carried out for 95 hours under the same conditions for these three different groups. At the end of the 95th hour, drug release was approximately 48% from non-coated PLGA NSs, approximately 40% from FBS coated PLGA NSs, and approximately 41% from human plasma coated PLGA NSs, respectively. This experiment, performed as triplicate, revealed that although the release of Dox was faster in the protein coated NSs during the first 47 hours, the release from NSs coated mostly with dysopsonins at the end of the 95th hour was almost similar to drug release from non-coated NSs. In addition, even though the protein types in the

HPC were different, the drug release from FBS coated or human plasma coated NSs was identical.

5. CONCLUSIONS AND OUTLOOK

5.1 Conclusions

In this thesis, different biodegradable PLGA and PCL NPs were synthesized to compare each other by miniemulsion/solvent evaporation technique. Non-ionic PVA was used as the surfactant, and olive oil was used for the NC synthesis. After the synesis and characterization, PC structure was formed around the NPs' surface by using human plasma or FBS. All experiments containing human plasma were conducted at Max Planck Institute for Polymer Research by approval of the local ethics committee "Landesärztekammer Rheinland-Pfalz" (Bearbeitungsnummer: 837.439.12 (8540-F)). Proteins in the PC structure were analyzed and their effect on drug release from PLGA NSs was investigated. The results obtained as a consequence of all experiments were as follows:

1. Using different organic solvents affected the size of NSs significantly. Ethyl acetate enabled to obtain of smaller-sized PLGA NSs because of its polarity.

2. Using different surfactants influenced the size and zeta potential of PLGA NCs. Ionic SDS ensured smaller-sized and more negatively charged PLGA NCs.

3. Keeping the ratios between polymer, surfactant, and olive oil constant; however, changing their amounts did not cause a significant difference in the size of the synthesized NCs.

4. Using the same ratios of the same surfactant and different biodegradable polymers did not result in a significant difference in the size of the synthesized NSs.

5. Creating core-shell morphology by adding olive oil led to an increase in size and PDI except using SDS as a surfactant. When SDS was used as the surfactant, the NCs had a smaller size and PDI than the size and PDI of NSs synthesized using PVA as the surfactant.

6. The images of TEM and SEM confirmed the PLGA NS or hollow capsule morphologies.

7. PCL NS or hollow capsule morphologies were verified by images of TEM and SEM.

8. Three times centrifugation showed that PLGA NCs synthesized using SDS were not redispersed in PBS or millipore water after the centrifugation. Therefore, they were not a suitable candidate for PC experiments despite being the smallest in size among the NCs.

9. Centrifugation also indicated that when PCL NSs were centrifuged at 20.000 g for 1 hour, they formed aggregates. Therefore, their centrifugation conditions were optimized at 15.000 g for 20 minutes. They did not form any aggregates after centrifugation under these conditions.

10. As a result of centrifugation, it was determined that PCL NCs did not remain stable at 15.000 g, 10.000 g, or 5000 g for 20 minutes, and their structures were broken.

11. PLGA and PCL NSs synthesized using chloroform were used in PC experiments to keep conditions the same even when the organic solvent was evaporated. The PC structure was constituted using human plasma or FBS. For comparison, a group of NSs was only treated with PBS. The size and PDI of both PLGA and PCL NSs were increased when treated with human plasma or FBS compared to the control group.

12. Protein assay showed that the concentration of proteins in the supernatants collected after each centrifugation gradually decreased from the SPC to the HPC. In addition, it revealed the difference in protein concentration in human plasma and protein concentration in FBS.

13. Proteins in the PC structure formed with either human plasma or FBS were separated according to their molecular weights by SDS-PAGE. SDS-PAGE confirmed that there was a decrease in the protein amounts after each centrifugation step.

14. There was a distinct band at 62 kDa in both human plasma and FBS HPC of PLGA and PCL which most likely referred to serum albumin.

15. However, there was more than one band of different low molecular weight proteins in the PLGA HPC formed by human plasma, while only one band in the 17-28 kDa range was seen in the FBS HPC of PLGA.

16. When the HPC of PCL was imaged by SDS-PAGE, it was observed that proteins with high molecular weight above 198 kDa formed more bands in the HPC of human plasma.

17. Liquid chromatography-mass spectrometry confirmed that serum albumin was the most abundant protein in the HPC structure of PLGA NSs formed by FBS and human plasma. Complement C3 and Apolipoprotein B-100 were the most abundant proteins in the HPC of human plasma after serum albumin, while Alpha-2-HS-glycoprotein and Alpha-1-antiproteinase were the second and third most abundant proteins in FBS HPC.

18. When all the proteins in the PLGA HPC were grouped, it was determined that the rate of the dysopsonin group was higher than the rate of the opsonin group in human plasma samples. However, their rates were similar in FBS samples.

19. Liquid chromatography-mass spectrometry results of PCL HPC showed that apolipoprotein E was the most abundant protein in the HPC of both FBS and human plasma. The second and third most abundant proteins were serum albumin and alpha-2-hs-glycoprotein in the FBS HPC; immunoglobulin heavy constant mu and immunoglobulin kappa constant in the human plasma HPC.

20. According to PCL HPC grouping, the proportion of dysopsonins in FBS samples was slightly higher than that of opsonins. On the other hand, the ratios of dysopsonin and opsonin were similar in the human plasma samples.

21. When Dox was encapsulated into PLGA, the size of PLGA NSs increased.

22. The zeta potential of Dox encapsulated PLGA NSs changed compared to their non-encapsulated conditions.

23. The drug loading amount was determined as 0.95 mg/mL.

24. Dox encapsulated PLGA NSs were centrifuged once and redispersed in 0.01 M pH 7.4 sodium phosphate buffer to determine their stability. The size and PDI of Dox-encapsulated PLGA NSs were quite similar to originated Dox encapsulated PLGA NSs.

25. The size and PDI of human plasma or FBS coated Dox encapsulated PLGA NSs were increased compared to the control group. However, their zeta potential was similar to each other.

26. The gel image of human plasma coated PLGA NSs and Dox encapsulated PLGA NSs was almost identical. In addition, FBS coated Dox encapsulated PLGA NSs had a similar gel image to FBS coated PLGA NSs. However, FBS coated PLGA NSs had a band in the range of 17-28 kDa, while this band was not observed in Dox encapsulated NSs.

27. The Dox release from protein coated NSs and non-coated NSs was almost identical. At the end of the 95th hour, Dox was released from non-coated, FBS coated, and human plasma coated PLGA NSs of approximately 48%, 40%, and 41%, respectively.

5.2 Outlook

Biodegradable PLGA and PCL NPs are important nanocarrier system candidates for the delivery of chemotherapeutic agents. In addition to the conducted studies, the release experiments of doxorubicin from PC coated and non-coated PCL NSs will be performed. Furthermore, paclitaxel, which is another important chemotherapeutic agent, will be encapsulated into PLGA and PCL NSs separately, followed by the performing the drug release experiments in the presence and absence of PC structure to investigate the effect of PC on drug release [73–75].

Drug release at pH 5.5 and 6.5 which are important pH values to mimic cancerous cells can be performed for PLGA or PCL NSs.

Internalization of nanospheres is one of the important points to determine the effect of the treatment. Cellular uptake studies of PC coated NSs and non-coated NSs will be carried out to identify the internalization of NSs.

REFERENCES

1. Gavas, S., S. Quazi and T. M. Karpiński, "Nanoparticles for Cancer Therapy: Current Progress and Challenges", *Nanoscale Research Letters*, Vol. 16, p. 173, 2021.

2. Dhaliwal Biomed Sci, K. J. and T. Res, "Biodegradable Polymers and their Role in Drug Delivery Systems", *Biomedical Journal of Scientific Technical Research*, Vol. 11, No. 1, pp. 001–006, 2018.

3. Martínez-Negro, M., G. González-Rubio, E. Aicart, K. Landfester, A. Guerrero-Martínez and E. Junquera, "Insights into colloidal nanoparticle-protein corona interactions for nanomedicine applications", *Advances in Colloid and Interface Science*, Vol. 289, p. 102366, mar 2021.

4. Jing, Z., Q. Du, X. Zhang and Y. Zhang, "Nanomedicines and nanomaterials for cancer therapy: Progress, challenge and perspectives", *Chemical Engineering Journal*, Vol. 446, p. 137147, oct 2022.

5. Siegel, R. L., K. D. Miller, H. E. Fuchs and A. Jemal, "Cancer statistics, 2022", *CA: A Cancer Journal for Clinicians*, Vol. 72, No. 1, pp. 7–33, jan 2022.

6. Pei, Z., S. Chen, L. Ding, J. Liu, X. Cui, F. Li and F. Qiu, "Current perspectives and trend of nanomedicine in cancer: A review and bibliometric analysis", *Journal of Controlled Release*, Vol. 352, pp. 211–241, dec 2022.

7. Liao, Z., S. W. Wong, H. L. Yeo and Y. Zhao, "Smart nanocarriers for cancer treatment: Clinical impact and safety", *NanoImpact*, Vol. 20, p. 100253, oct 2020.

8. Yao, Y., Y. Zhou, L. Liu, Y. Xu, Q. Chen, Y. Wang, S. Wu, Y. Deng, J. Zhang and A. Shao, "Nanoparticle-Based Drug Delivery in Cancer Therapy and Its Role in Overcoming Drug Resistance", *Frontiers in Molecular Biosciences*, Vol. 7, p. 193, aug 2020.

9. Shi, J., A. R. Votruba, O. C. Farokhzad and R. Langer, "Nanotechnology in Drug Delivery and Tissue Engineering: From Discovery to Applications", *Nano letters*, Vol. 10, No. 9, p. 3223, sep 2010.

10. Soares, S., J. Sousa, A. Pais and C. Vitorino, "Nanomedicine: Principles, properties, and regulatory issues", *Frontiers in Chemistry*, Vol. 6, No. AUG, p. 360, aug 2018.

11. Din, F. U., W. Aman, I. Ullah, O. S. Qureshi, O. Mustapha, S. Shafique and A. Zeb, "Effective use of nanocarriers as drug delivery systems for the treatment of selected tumors", *International Journal of Nanomedicine*, Vol. 12, p. 7291, oct 2017.

12. Mi, P., "Stimuli-responsive nanocarriers for drug delivery, tumor imaging, therapy and theranostics", *Theranostics*, Vol. 10, No. 10, p. 4557, 2020.

13. Zielinska, A., F. Carreiró, A. M. Oliveira, A. Neves, B. Pires, D. Nagasamy Venkatesh, A. Durazzo, M. Lucarini, P. Eder, A. M. Silva, A. Santini and E. B. Souto, "Polymeric Nanoparticles: Production, Characterization, Toxicology and Ecotoxicology", *Molecules*, Vol. 25, No. 16, aug 2020.

14. Gagliardi, A., E. Giuliano, E. Venkateswararao, M. Fresta, S. Bulotta, V. Awasthi and D. Cosco, "Biodegradable Polymeric Nanoparticles for Drug Delivery to Solid Tumors", *Frontiers in Pharmacology*, Vol. 12, feb 2021.

15. Singh, R. and J. W. Lillard, "Nanoparticle-based targeted drug delivery", *Experimental and Molecular Pathology*, Vol. 86, No. 3, pp. 215–223, jun 2009.

16. Sabourian, P., G. Yazdani, S. S. Ashraf, M. Frounchi, S. Mashayekhan, S. Kiani and A. Kakkar, "Effect of Physico-Chemical Properties of Nanoparticles on Their Intracellular Uptake", *International journal of molecular sciences*, Vol. 21, No. 21, pp. 1–20, nov 2020.

17. Yagublu, V., A. Karimova, J. Hajibabazadeh, C. Reissfelder, M. Muradov, S. Bellucci and A. Allahverdiyev, "Overview of Physicochemical Properties of Nanoparticles as Drug Carriers for Targeted Cancer Therapy", *Journal of functional biomaterials*, Vol. 13, No. 4, p. 196, oct 2022.

18. Patra, J. K., G. Das, L. F. Fraceto, E. V. R. Campos, M. D. P. Rodriguez-Torres, L. S. Acosta-Torres, L. A. Diaz-Torres, R. Grillo, M. K. Swamy, S. Sharma, S. Habtemariam and H. S. Shin, "Nano based drug delivery systems: recent developments and future prospects", *Journal of Nanobiotechnology 2018 16:1*, Vol. 16, No. 1, pp. 1–33, sep 2018.

19. Attia, M. F., N. Anton, J. Wallyn, Z. Omran and T. F. Vandamme, "An overview of active and passive targeting strategies to improve the nanocarriers efficiency to tumour sites", *Journal of Pharmacy and Pharmacology*, Vol. 71, No. 8, pp. 1185–1198, aug 2019.

20. Rajani, C., P. Borisa, T. Karanwad, Y. Borade, V. Patel, K. Rajpoot and R. K. Tekade, "Cancer-targeted chemotherapy: Emerging role of the folate anchored dendrimer as drug delivery nanocarrier", *Pharmaceutical Applications of Dendrimers*, pp. 151–198, jan 2020.

21. Shukla, T., N. Upmanyu, S. P. Pandey and M. S. Sudheesh, "Site-specific drug delivery, targeting, and gene therapy", *Nanoarchitectonics in Biomedicine*, pp. 473–505, jan 2019.

22. Yoo, J., C. Park, G. Yi, D. Lee and H. Koo, "Active Targeting Strategies Using Biological Ligands for Nanoparticle Drug Delivery Systems", *Cancers 2019, Vol. 11, Page 640*, Vol. 11, No. 5, p. 640, may 2019.

23. Jasim, A., S. Abdelghany and K. Greish, "Current Update on the Role of Enhanced Permeability and Retention Effect in Cancer Nanomedicine", *Nanotechnology-Based Approaches for Targeting and Delivery of Drugs and Genes*, pp. 62–109, jan 2017.

24. Gavasane, A. J., "Synthetic Biodegradable Polymers Used in Controlled Drug Delivery System: An Overview", *Clinical Pharmacology Biopharmaceutics*, Vol. 3, No. 2, 2014.

25. Jazayeri, H. E., S. M. Lee, L. Kuhn, F. Fahimipour, M. Tahriri and L. Tayebi, "Polymeric scaffolds for dental pulp tissue engineering: A review", *Dental materials*

: official publication of the Academy of Dental Materials, Vol. 36, No. 2, pp. e47–e58, feb 2020.

26. Abbasian, M., B. Massoumi, R. Mohammad-Rezaei, H. Samadian and M. Jaymand, "Scaffolding polymeric biomaterials: Are naturally occurring biological macromolecules more appropriate for tissue engineering?", *International Journal of Biological Macromolecules*, Vol. 134, pp. 673–694, aug 2019.

27. Hasnain, M. S., S. A. Ahmad, N. Chaudhary, M. N. Hoda and A. K. Nayak, "Biodegradable polymer matrix nanocomposites for bone tissue engineering", *Applications of Nanocomposite Materials in Orthopedics*, pp. 1–37, Elsevier, nov 2018.

28. Tariverdian, T., T. Navaei, P. B. Milan, A. Samadikuchaksaraei and M. Mozafari, "Functionalized polymers for tissue engineering and regenerative medicines", *Advanced Functional Polymers for Biomedical Applications*, pp. 323–357, Elsevier, 2019.

29. Zhu, M., A. K. Whittaker, F. Y. Han and M. T. Smith, "Journey to the Market: The Evolution of Biodegradable Drug Delivery Systems", *Applied Sciences 2022, Vol. 12, Page 935*, Vol. 12, No. 2, p. 935, jan 2022.

30. Su, S. and P. M. Kang, "Systemic Review of Biodegradable Nanomaterials in Nanomedicine", *Nanomaterials*, Vol. 10, No. 4, apr 2020.

31. Lanao, R. P., A. M. Jonker, J. G. Wolke, J. A. Jansen, J. C. Van Hest and S. C. Leeuwenburgh, "Physicochemical Properties and Applications of Poly(lactic-co-glycolic acid) for Use in Bone Regeneration", *Tissue Engineering. Part B, Reviews*, Vol. 19, No. 4, p. 380, aug 2013.

32. Kumari, A., S. K. Yadav and S. C. Yadav, "Biodegradable polymeric nanoparticles based drug delivery systems", *Colloids and Surfaces B: Biointerfaces*, Vol. 75, No. 1, pp. 1–18, jan 2010.

33. Song, R., M. Murphy, C. Li, K. Ting, C. Soo and Z. Zheng, "Current development of biodegradable polymeric materials for biomedical applications", *Drug Design, Development and Therapy*, pp. 12–3117, 2018.

34. Chittasupho, C., K. Lirdprapamongkol, P. Kewsuwan and N. Sarisuta, "Targeted delivery of doxorubicin to A549 lung cancer cells by CXCR4 antagonist conjugated PLGA nanoparticles", *European journal of pharmaceutics and biopharmaceutics : official journal of Arbeitsgemeinschaft fur Pharmazeutische Verfahrenstechnik e.V*, Vol. 88, No. 2, pp. 529–538, 2014.

35. Anselmo, A. C. and S. Mitragotri, "Nanoparticles in the clinic: An update", *Bioengineering Translational Medicine*, Vol. 4, No. 3, sep 2019.

36. Chatterjee, M. and N. Chanda, "Formulation of PLGA nano-carriers: specialized modification for cancer therapeutic applications", *Materials Advances*, Vol. 3, No. 2, pp. 837–858, jan 2022.

37. Nair, L. S. and C. T. Laurencin, "Biodegradable polymers as biomaterials", *Progress in Polymer Science*, Vol. 32, No. 8-9, pp. 762–798, aug 2007.

38. Karlsson, J., H. J. Vaughan and J. J. Green, "Biodegradable Polymeric Nanoparticles for Therapeutic Cancer Treatments", *Annual review of chemical and biomolecular engineering*, Vol. 9, p. 105, jun 2018.

39. Pappalardo, D., T. Mathisen and A. Finne-Wistrand, "Biocompatibility of Resorbable Polymers: A Historical Perspective and Framework for the Future", *Biomacromolecules*, Vol. 20, No. 4, pp. 1465–1477, apr 2019.

40. Li, H., Y. Wang, Q. Tang, D. Yin, C. Tang, E. He, L. Zou and Q. Peng, "The protein corona and its effects on nanoparticle-based drug delivery systems", *Acta biomaterialia*, Vol. 129, pp. 57–72, jul 2021.

41. Digiacomo, L., D. Pozzi, S. Palchetti, A. Zingoni and G. Caracciolo, "Impact of the protein corona on nanomaterial immune response and targeting ability", *Wiley Interdisciplinary Reviews: Nanomedicine and Nanobiotechnology*, Vol. 12, No. 4, p. e1615, jul 2020.

42. Wolfram, J., Y. Yang, J. Shen, A. Moten, C. Chen, H. Shen, M. Ferrari and Y. Zhao, "The nano-plasma interface: Implications of the protein corona", *Colloids and Surfaces B: Biointerfaces*, Vol. 124, pp. 17–24, dec 2014.

43. Nguyen, V. H. and B. J. Lee, "Protein corona: a new approach for nanomedicine design", *International Journal of Nanomedicine*, Vol. 12, p. 3137, apr 2017.

44. Agrawal, N., M. Mahendra, T. Singh and B. Gangil, "Nanobiology in medicine", *Nanomedicine Manufacturing and Applications*, pp. 57–71, jan 2021.

45. Sempf, K., T. Arrey, S. Gelperina, T. Schorge, B. Meyer, M. Karas and J. Kreuter, "Adsorption of plasma proteins on uncoated PLGA nanoparticles", *European Journal of Pharmaceutics and Biopharmaceutics*, Vol. 85, No. 1, pp. 53–60, sep 2013.

46. Wang, X. and W. Zhang, "The Janus of Protein Corona on nanoparticles for tumor targeting, immunotherapy and diagnosis", *Journal of Controlled Release*, Vol. 345, pp. 832–850, may 2022.

47. Rampado, R., S. Crotti, P. Caliceti, S. Pucciarelli and M. Agostini, "Recent Advances in Understanding the Protein Corona of Nanoparticles and in the Formulation of "Stealthy" Nanomaterials", *Frontiers in Bioengineering and Biotechnology*, Vol. 8, p. 166, apr 2020.

48. Li, Y. and J. S. Lee, "Insights into Characterization Methods and Biomedical Applications of Nanoparticle–Protein Corona", *Materials*, Vol. 13, No. 14, jul 2020.

49. Vianello, F., A. Cecconello and M. Magro, "Toward the Specificity of Bare Nanomaterial Surfaces for Protein Corona Formation", *International Journal of Molecular Sciences*, Vol. 22, No. 14, jul 2021.

50. Akhter, M. H., H. Khalilullah, M. Gupta, M. A. Alfaleh, N. A. Alhakamy, Y. Riadi and S. Md, "Impact of Protein Corona on the Biological Identity of Nanomedicine: Understanding the Fate of Nanomaterials in the Biological Milieu.", *Biomedicines*, Vol. 9, No. 10, pp. 1496–1496, oct 2021.

51. García-álvarez, R. and M. Vallet-Regí, "Hard and Soft Protein Corona of Nanomaterials: Analysis and Relevance", *Nanomaterials 2021, Vol. 11, Page 888*, Vol. 11, No. 4, p. 888, mar 2021.

52. Papini, E., R. Tavano and F. Mancin, "Opsonins and Dysopsonins of Nanoparticles: Facts, Concepts, and Methodological Guidelines", *Frontiers in Immunology*, Vol. 11, p. 2343, oct 2020.

53. Francia, V., R. M. Schiffelers, P. R. Cullis and D. Witzigmann, "The Biomolecular Corona of Lipid Nanoparticles for Gene Therapy", *Bioconjugate Chemistry*, Vol. 31, No. 9, pp. 2046–2059, sep 2020.

54. Bilardo, R., F. Traldi, A. Vdovchenko and M. Resmini, "Influence of surface chemistry and morphology of nanoparticles on protein corona formation", *Wiley Interdisciplinary Reviews: Nanomedicine and Nanobiotechnology*, Vol. 14, No. 4, jul 2022.

55. Shah, J. and S. Singh, "CHAPTER 1 Nanoparticle–Protein Corona Complex: Composition, Kinetics, Physico–Chemical Characterization, and Impact on Biomedical Applications", *Issues in Toxicology*, Vol. 2019-Janua, No. 40, pp. 1–30, 2019.

56. Huang, W., G. Xiao, Y. Zhang and W. Min, "Research progress and application opportunities of nanoparticle–protein corona complexes", *Biomedicine Pharmacotherapy*, Vol. 139, p. 111541, jul 2021.

57. Mishra, R. K., A. Ahmad, A. Vyawahare, P. Alam, T. H. Khan and R. Khan, "Biological effects of formation of protein corona onto nanoparticles", *International Journal of Biological Macromolecules*, Vol. 175, pp. 1–18, apr 2021.

58. Quagliarini, E., L. Digiacomo, S. Renzi, D. Pozzi and G. Caracciolo, "A decade of the liposome-protein corona: Lessons learned and future breakthroughs in theranostics", *Nano Today*, Vol. 47, p. 101657, dec 2022.

59. Iyisan, B., R. Thiramanas, N. Nazarova, Y. Avlasevich, V. Mailänder, S. Baluschev and K. Landfester, "Temperature Sensing in Cells Using Polymeric Upconversion Nanocapsules", *Biomacromolecules*, Vol. 21, No. 11, pp. 4469–4478, nov 2020.

60. Musyanovych, A., J. Schmitz-Wienke, V. Mailänder, P. Walther and K. Landfester, "Preparation of biodegradable polymer nanoparticles by miniemulsion technique

and their cell interactions", *Macromolecular bioscience*, Vol. 8, No. 2, pp. 127–139, feb 2008.

61. Park, J., P. M. Fong, J. Lu, K. S. Russell, C. J. Booth, W. M. Saltzman and T. M. Fahmy, "PEGylated PLGA nanoparticles for the improved delivery of doxorubicin", *Nanomedicine : nanotechnology, biology, and medicine*, Vol. 5, No. 4, pp. 410–418, dec 2009.

62. Iyisan, B., J. Simon, Y. Avlasevich, S. Baluschev, V. Mailaender and K. Landfester, "Antibody-Functionalized Carnauba Wax Nanoparticles to Target Breast Cancer Cells", *ACS Applied Bio Materials*, Vol. 5, No. 2, pp. 622–629, feb 2022.

63. Li, M., S. Jiang, J. Simon, D. Paßlick, M. L. Frey, M. Wagner, V. Mailander, D. Crespy and K. Landfester, "Brush conformation of polyethylene glycol determines the stealth effect of nanocarriers in the low protein adsorption regime", *Nano Letters*, Vol. 21, No. 4, pp. 1591–1598, feb 2021.

64. Ndumiso, M., N. Buchtová, L. Husselmann, G. Mohamed, A. Klein, M. Aucamp, D. Canevet, S. D'Souza, R. E. Maphasa, F. Boury and A. Dube, "Comparative whole corona fingerprinting and protein adsorption thermodynamics of PLGA and PCL nanoparticles in human serum", *Colloids and Surfaces B: Biointerfaces*, Vol. 188, p. 110816, apr 2020.

65. Shahabi, S., L. Treccani, R. Dringen and K. Rezwan, "Utilizing the protein corona around silica nanoparticles for dual drug loading and release", *Nanoscale*, Vol. 7, No. 39, pp. 16251–16265, oct 2015.

66. Simon, J., L. K. Müller, M. Kokkinopoulou, I. Lieberwirth, S. Morsbach, K. Landfester and V. Mailänder, "Exploiting the biomolecular corona: pre-coating of nanoparticles enables controlled cellular interactions", *Nanoscale*, Vol. 10, No. 22, pp. 10731–10739, jun 2018.

67. Oberländer, J., C. Champanhac, R. da Costa Marques, K. Landfester and V. Mailänder, "Temperature, concentration, and surface modification influence the cellular uptake and the protein corona of polystyrene nanoparticles", *Acta Biomaterialia*, Vol. 148, pp. 271–278, aug 2022.

68. Oberländer, J., R. Ayerbe, J. Cabellos, R. da Costa Marques, B. Li, N. Günday-Türeli, A. E. Türeli, R. Ofir, E. I. Shalom and V. Mailänder, "Higher Loading of Gold Nanoparticles in PAD Mesenchymal-like Stromal Cells Leads to a Decreased Exocytosis", *Cells*, Vol. 11, No. 15, p. 2323, aug 2022.

69. Kokkinopoulou, M., J. Simon, K. Landfester, V. Mailänder and I. Lieberwirth, "Visualization of the protein corona: towards a biomolecular understanding of nanoparticle-cell-interactions", *Nanoscale*, Vol. 9, No. 25, pp. 8858–8870, jun 2017.

70. Silva, J. C., M. V. Gorenstein, G. Z. Li, J. P. Vissers and S. J. Geromanos, "Absolute quantification of proteins by LCMSE: a virtue of parallel MS acquisition", *Molecular cellular proteomics : MCP*, Vol. 5, No. 1, pp. 144–156, jan 2006.

71. Iyisan, B., J. Kluge, P. Formanek, B. Voit and D. Appelhans, "Multifunctional and Dual-Responsive Polymersomes as Robust Nanocontainers: Design, Formation by Sequential Post-Conjugations, and pH-Controlled Drug Release", *Chemistry of Materials*, , No. 5, pp. 1513–1525, mar 2016.

72. Hussain, M. H., N. F. Abu Bakar, A. N. Mustapa, K. F. Low, N. H. Othman and F. Adam, "Synthesis of Various Size Gold Nanoparticles by Chemical Reduction Method with Different Solvent Polarity", *Nanoscale Research Letters*, Vol. 15, No. 1, pp. 1–10, jul 2020.

73. Yu, D. L., Z. P. Lou, F. Y. Ma and M. Najafi, "The interactions of paclitaxel with tumour microenvironment", *International Immunopharmacology*, Vol. 105, p. 108555, apr 2022.

74. Ünal, S., O. Doğan, Y. Aktaş and S. Yazar, "Paclitaxel-Loaded Polycaprolactone Nanoparticles For Lung Tumors; Formulation, Comprehensive in Vitro Characterization and Release Kinetic Studies", *J. Fac. Pharm. Ankara / Ankara Ecz. Fak. Derg*, Vol. 46, No. 3, pp. 1009–1029, 2022.

75. Fonseca, C., S. Simões and R. Gaspar, "Paclitaxel-loaded PLGA nanoparticles: preparation, physicochemical characterization and in vitro anti-tumoral activity", *Journal of Controlled Release*, Vol. 83, No. 2, pp. 273–286, oct 2002.

APPENDIX A. CALIBRATION CURVE FOR PROTEIN ASSAY

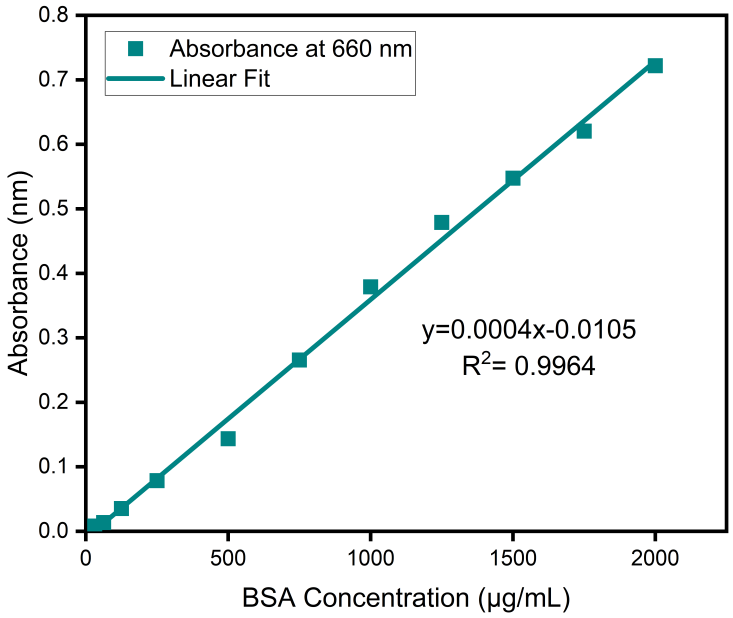

Figure A.1: Calibration Curve of BSA determined from absorbance values at λ=660 nm, measured in millipore H_2O

APPENDIX B. CALIBRATION CURVE FOR DRUG RELEASE

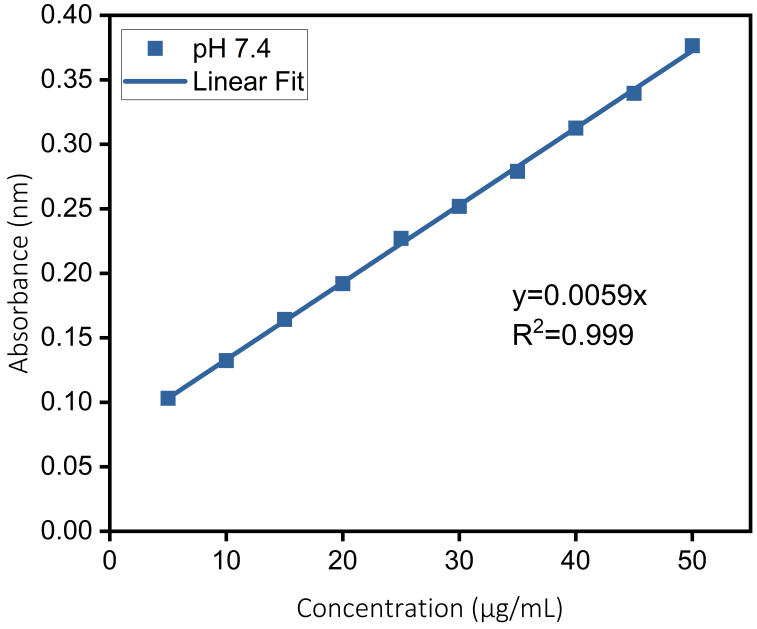

Figure B.1: Calibration Curve of Doxorubicin at pH 7.4 and determined from absorbance values at λ=480 nm